NUMBER OF STORMS IN SEVERAL RUSSIAN SEAS: TRENDS AND CONNECTION TO LARGE-SCALE ATMOSPHERIC INDICES

Stanislav Myslenkov[1,2,3]*, Elizaveta Kruglova[1,2], Alisa Medvedeva[1,2], Ksenia Silvestrova[2], Victor Arkhipin[1], Adem Akpinar[4] and Sergey Dobrolyubov[1]

[1] Lomonosov Moscow State University, Moscow, Russia
[2] Shirshov Institute of Oceanology RAS, Moscow, Russia
[3] Hydrometeorological Research Centre of the Russian Federation, Moscow, Russia
[4] Bursa Uludag University, Department of Civil Engineering, Bursa, Turkey
* **Correspondence to:** Stanislav Myslenkov, stasocean@gmail.com

Abstract: The main motivation of this research is to assess the trends of storm recurrence for the time period from 1979 up to 2020 and to analyze the connection between storminess and large-scale atmospheric circulation indices. This research contains information about the number of storms that occurred in seven Russian Seas, including the Black, Caspian, Barents, Kara, Bering Seas, the Sea of Okhotsk and the Sea of Japan/East Sea. The analysis of wave climate and storm activity is based on the results of wave modeling by WAVEWATCH III with input NCEP/CFSR wind and ice data. The long-term significant wave height (SWH) maximum is 15.5 m in the Sea of Okhotsk and 16.5 m in the Bering Sea. Significant linear basin-wide positive trends in the number of storms were found in the Kara, Caspian, Bering, Okhotsk Seas, and in the Sea of Japan. The weak positive correlation was found only between the number of storms and North Pacific index in the Bering Sea and between the number of storms and Arctic oscillation index in the Barents Sea. For other seas, it is no connections between number of storms and large-scale atmospheric indices, therefore, storm activity in the inner and semi-closed seas is regulated by the local wind and ice conditions, basin orography and bathymetry.

Keywords: wind waves; wave modeling; number of storms; trend; atmospheric indices

RESEARCH ARTICLE

1. Introduction

Wind wave modeling for long periods helps to understand climate changes on Earth that occurred in the past, and to improve their forecast in the future. Coastal and marine infrastructures are most vulnerable during storms, so it is important to study seasonal and interannual variability of sea storms.

Wind waves are being studied by numerous methods with the use of different sources and approaches [*Amarouche and Akpınar*, 2021, *Cavaleri et al.*, 2007, *Divinsky and Kuklev*, 2022, *Young and Ribal*, 2019]. Direct wave measurements is usually sparse and altimetry data often has rough temporal resolution [*Young and Ribal*, 2019]. Meanwhile, numerical modeling allows to obtain long-time and wide-spatial coverage data of different wind wave parameters.

Mean and extreme characteristics of wind waves for all Russian seas are given in the Wind and Wave Climate Handbooks [*Lopatoukhin et al.*, 2003, 2006, 2009, 2010]. The data are based on the results of modeling, but it need to be improved and updated by the latest atmospheric reanalysis and detailed computational grid.

Stopa et al. [2016] showed the main features of the wave climate and trends in the Arctic region for the 1992–2014 period based on altimetry data and wave hindcast results. The reduction of the sea ice coverage caused a growth of wave heights. However, regional trends in the Arctic were influenced by large-scale interannual climate oscillations such as the North Atlantic Oscillation (NAO) and the Pacific Decadal Oscillation (PDO) [*Stopa et al.*, 2016]. Changes in the ice-free period it the Arctic confirmed by satellite observations [*Smirnov et al.*, 2021]. *Ogorodov et al.* [2020] showed that increase in the duration of the ice-free period combined with wind-wave activity intensification would accelerate the retreat of the Arctic coastline. The thermoabrasion potential has been significantly increasing in recent years in the Russian Arctic [*Ogorodov et al.*, 2022]. There is a strong variability of turbulent heat fluxes in the Russian Arctic [*Surkova and Romanenko*, 2021] and their relationship with changes in storm activity for the Barents Sea is considered in [*Myslenkov et al.*, 2021a]. The sea ice marginal zone has influence for the turbulent heat fluxes in Arctic [*Selivanova et al.*, 2021]. *Liu et al.* [2016] uses satellite observations to study wave climatology in the Arctic Ocean in summer. Wind speeds and wave heights in the Barents and Kara Seas initially increased from 1996 to 2006 and later decreased until 2015. Wave heights in the Chukchi, Beaufort and Laptev Seas had been increasing by 0.1 up to 0.3 m per decade [*Liu et al.*, 2016]. On the contrary, the trends of wave heights in the Greenland and Barents Seas were weak and not statistically significant. Winds and waves increased between 1996 and 2006 in the Barents and Kara Seas. Large-scale atmospheric circulation variations such as the Arctic Oscillation (AO) had an impact on the variation of winds and waves in the Atlantic sector [*Liu et al.*, 2016]. The total significant wave height (SWH) in the Nordic Seas are mostly due to swell and to the wave propagation effect [*Semedo et al.*, 2014]. Inter-annual variations of the mean and extreme SWH in the Kara Sea are described in [*Duan et al.*, 2019]. Positive trends of the highest SWH and wind speed are shown for the Laptev and Beaufort Seas in *Waseda et al.* [2018]. *Wang and Swail* [2001] identified significant trends in seasonal extreme SWH for the North Atlantic and for the North Pacific. The number of storms with SWH ≥ 7 m in winter has a correlation with the AO for the Barents Sea [*Myslenkov et al.*, 2019]. High recurrence of strong winds and the reducing of sea ice lead to the increase of number of storms in the Kara Sea [*Myslenkov et al.*, 2021a].

There is also important research work on wave heights in the future climate projections [*Casas-Prat et al.*, 2018, *Dobrynin et al.*, 2012, *Morim et al.*, 2020]. Arctic Ocean Wave climate in 21st century presented here [*Khon et al.*, 2014]. In the future climate there is a high probability of an increase of the wave height in the Norwegian and the Barents Seas [*Aarnes et al.*, 2017].

As for the Black Sea, *Divinsky and Kosyan* [2020] reveal the increase of the average wave power (PW) in the northeastern and, partially, in the central part of the sea. *Akpınar et al.* [2019] found a decreasing trend in mean wave energy flux and an increasing trend of maximum PW at most of the investigated stations of the Black Sea. These results correlate with various studies regarding the Black Sea [*Lin-Ye et al.*, 2018, *Onea and Rusu*, 2017, *Rusu*, 2015]. *Aydoğan and Ayat* [2018] showed the correlation of annual mean SWH and 95% percentile SWH with AO and AMO (Atlantic multidecadal oscillation) indices. SWH in the north and northwestern parts of the Black Sea are negatively correlated with the AO, while SWH in the eastern parts are positively correlated with the AMO teleconnection pattern. *Kislov et al.* [2016] showed that the frequency of storm conditions in the Black and Caspian seas would increase accordingly to the predicted variations of air temperature, precipitation, wind speed and other meteorological parameters in the 21st century (RCP8.5 scenario).

Wave climate of the Caspian Sea based on NCEP/NCAR reanalysis presented in studies of [*Lopatoukhin*, 2019, *Lopatukhin and Yaitskaya*, 2018, *Yaitskaya*, 2017]. The main features of the wave climate in the Caspian Sea based on altimetry data are displayed in [*Kudryavtseva et al.*, 2019, *Lama et al.*, 2022]. The wave energy was estimated in [*Amini et al.*, 2021, *Kamranzad et al.*, 2016]. The maximum SWH was 8.2 m based on wave hindcast [*Pavlova et al.*, 2022]. Some studies presented the results of wind waves analysis for the

Caspian Sea [*Amirinia et al.*, *2017*, *Imrani et al.*, *2022*]. However, the wave climate and storm activities have not been properly investigated.

The decadal fluctuations and strong El Niño's had a strong influence on long-term trends in storm intensity in the North Pacific [*Bromirski et al.*, *2013*]. The upward trends in SWH and PW were found especially in winter. The maximum PW was associated with an increase in wave activity during the warm phase of the PDO. Importantly, the hindcast shows a recent decrease in PW in much of the North Pacific, in contrast to the long-term increase in PW and SWH. This recent decrease was associated with the prevalent PDO cool phase that developed after the late 1990s [*Bromirski et al.*, *2013*]. *Mei and Xie* [*2016*] showed the intensification by 12–15% for typhoons that strike East and Southeast Asia for the past 37 years. Category 4 and 5 storms have doubled or even tripled [*Mei and Xie*, *2016*]. High correlation between winter averaged wave height and different atmospheric indices were found in North Atlantic and North Pacific [*Shimura et al.*, *2013*].

WW3 and SWAN models were implemented to forecast wind waves parameters in the Far Eastern Seas and North Pacific [*Vrazhkin*, *2013*]. *Lyubitskiy et al.* [*2021*] described a marine hazard in the Sea of Okhotsk. *Lopatoukhin et al.* [*2009*] showed the possible 9.9 m SWH can occur in the East/Japan Sea (EJS) once for 25 year. In winter, winds are strong due to the east Asian monsoon, while blowing mild or moderate and variable in summer [*Lee et al.*, *2010*]. In winter, atmospheric low pressure reacting with and passing through the EJS can sometimes cause abnormal storm waves on the Korean and Japanese coasts of the EJS. Storm waves and on their generation process and hindcast based on literature review and numerical modeling presented [*Lee et al.*, *2010*]. *Iwasaki and Otsuka* [*2021*] valuated WW3 wave-ice parameterization models using buoy measurements for the sea of Okhotsk. *Sasaki* [*2012*] estimated that the annual mean wave energy around Japan is $6.4\,\mathrm{kW\,m^{-1}}$, with an increasing trend. Although the increasing trend was only 4.2% relative to the annual mean, the author found a noticeable increasing trend in the wave energy on the east coast of Japan, which is related to the growing trend in surface wind speed east of Japan. Some information about ice, wind and waves trends is presented in [*Sharmar and Markina*, *2021*]. A high-resolution wave climate hindcast along the Japanese coast is presented in [*Shimura and Mori*, *2019*].

Number of storms analysis has been implemented for different basins [*de León and Soares*, *2015*, *Morales-Márquez et al.*, *2020*, *Rusu et al.*, *2015*]. The interannual variability and their connection with global atmospheric circulation are well described for the Mediterranean Sea [*Amarouche et al.*, *2022*].

We considered seven Russian seas in our research: two inland seas (the Black and Caspian Seas), two Arctic seas (the Barents and Kara seas), and three Far Eastern seas (the EJS, the Okhotsk and Bering seas), with the focus on the number of storms and their trends. We used the WW3 model and unstructured mesh. The main goal was to analyze the interannual variation of the number of storms for 40-year period from 1979 and its connection to large-scale atmospheric indices.

2. Data and Methods

2.1. Model Description and Configuration

Wind wave characteristics were calculated using the WW3 6.07 wave model [*Tolman*, *2019*]. The WW3 model considers wind speed, ice concentration, physical effects described below. A numerical solution of the wave action density spectrum equation is based on:

$$\frac{DN}{Dt} = \frac{S}{\sigma},$$

where $N(k,\theta) \equiv F(k,\theta)/\sigma$, k – wave number, θ – propagation direction, σ – relative frequency, D/Dt represents the total derivative and S represents the net effect of sources and sinks for the spectrum F [*Tolman*, *2019*]. S is a source function that describes the energy transfer from the wind to the waves, nonlinear wave interactions, and energy dissipation through the collapse of the crests at a great depth and in the coastal zone, friction against

the bottom and ice, wave scattering by ground relief forms, and reflection from the coast-line and floating objects. The energy balance equation is integrated using finite-difference schemes by the geographic grid and the wave parameters spectrum.

The calculations were made using ST6 scheme [*Zieger et al.*, 2015]. A discrete interaction approximation model was used for the possible nonlinear interactions of the waves. The approach of *Battjes and Janssen* [1978] was used for the wave height growth with the depth decrease in shallow water and for the related wave breaking with critical steepness value. The standard Joint North Sea Wave Observation Project scheme was used for bottom friction. The model spectral resolution is 36 directions (10°), the frequency range includes 36 intervals from 0.03 to 0.843 Hz. The time step for the integration of the complete wave action equation is 15 min. The time increment for the spectral energy transfer is 450 s. The time step for the integration of the source terms is dynamically adjusted for each separate grid point and global time step [*Tolman*, 2019].

The influence of sea ice on the waves is calculated due to the ICE0 scheme. A grid point is considered as ice-covered when ice concentration is > 0.5. We have carried out several tests for the Barents Sea previously and found that quality of the wave modeling in general is independent to the ice scheme choice. Differences were observed only in a narrow strip ~ 50 km near the ice edge. This aspect is not fundamental for the purpose of our study (long-term trends of the number of storms). We use the same model settings and time step for the all studied seas.

More detailed description of the model configuration, the main results were presented in [*Myslenkov et al.*, 2021a, *Platonov et al.*, 2022].

2.2. Data

The input data of the wind speed at 10 m and the sea ice concentration were taken from the NCEP/CFSR for the period from 1979 to 2010. This reanalysis has a spatial resolution $0.3° \times 0.3°$ and a time step of 1 hour (https://rda.ucar.edu/datasets/ds093.2). Since 2011, we have been using NCEP/CFSv2 with spatial resolution $\sim 0.205° \times 0.204°$ (https://rda.ucar.edu/datasets/ds094.1). The CFSv2 sea ice component includes a sea ice model and a simple assimilation scheme. We also used the wind data from the reanalysis ERA5 (https://cds.climate.copernicus.eu) with spatial resolution $0.25° \times 0.25°$.

There are many articles where we read about comparing of the wind wave quality based on ERA5 and CFSR/CFSv2 reanalysis. In one region ERA5 reanalysis is better for other region another [*Amarouche and Akpınar*, 2021, *Sharmar and Markina*, 2021, *Stefanakos*, 2021]. The SWAN model using CFSR winds shows lower bias in the hindcast SWH in the Black Sea, but in case ERA5 forcing it shows higher correlation coefficient [*Çalışır et al.*, 2021]. Therefore, we decided to provide an additional SWH calculation based on CFSR/CFSv2 and ERA5 reanalysis.

Wave simulations have been performed using unstructured grids for all studied seas (Figure 1). The spatial resolution was 10–20 km in the central open areas of the seas and 700–1000 m in the coastal zones. The unstructured grid for the Barents and Kara Seas included the North Atlantic region. North Pacific was included for the Far East Seas (Figure 1). This unstructured mesh allows to get a high spatial resolution not only in coastal zones, but in the narrow straits too. Wave energy can freely pass from the Pacific Ocean through the straits of the Kuril chain and Aleutian Islands when an unstructured mesh is used. The computational grids were created on the basis of the General Bathymetric Chart of the Oceans (GEBCO), which has a spatial resolution of ~ 1.85 km for deep sea. The bathymetry data used were updated for coastal zones by digitized navigation maps with spatial resolution 200–300 m.

We used only calm wave conditions on the open boundary. Sensitivity tests show that the open boundary in the central part of the Atlantic Ocean does not influence the waves in the Barents Sea at all [*Myslenkov et al.*, 2015]. There is an open boundary in the north for the Barents and Kara Seas, but there is sea ice there almost at all times [*Myslenkov et al.*, 2021a]. Wave energy passes weakly through narrow straits, so we expect that the open

boundary in the Vilkitsky Strait and in the Bering Strait does not have a great influence on the number of storms.

2.3. Model Quality Assessment

To assess model quality, we used buoy and satellite SWH data. The model quality validation presented for the Kara Sea [*Myslenkov et al.*, 2021b], the Barents Sea [*Myslenkov et al.*, 2021a], the Caspian Sea [*Myslenkov et al.*, 2018b] and the Black Sea [*Gippius and Myslenkov*, 2020] (Table 1). For the Bering Sea, modeled and measured data were compared with NOAA station (57°0′56″N, 177°42′11″W) for years 2018–2019 (totally 4583 samples) [https://www.ndbc.noaa.gov/station_history.php?station=46035]. This comparison has not been published before, so we put it in results section (Figure 3).

Table 1. Basic statistical parameters of model quality assessments

Sea	R	Bias (m)	RMSE (m)	SI	N	Reference
Kara	0.89 −0.93	(−0.03)–(−0.14)	0.32–0.38	0.24–0.28	∼ 190,000	ST6 configuration, Cryosat, Sentinel, Saral [*Myslenkov et al.*, 2021a,b]
Kara	0.94	0,07	0.32	0.28	400	Buoy data [*Myslenkov et al.*, 2021a,b]
Barents	0.88	0.04	0.53	0.28	∼ 266,000	CryoSat [*Myslenkov et al.*, 2021a,b]
Black	0.85	−0.11	0.36	0.36	∼ 61,000	Saral [*Gippius and Myslenkov*, 2020]
Black	0.76	−0.11	0.39	0.65	∼ 10,000	Buoy data [*Gippius and Myslenkov*, 2020]
Caspian	0.91	0.07	0.29	0.29	∼ 35,000	Saral [*Myslenkov et al.*, 2018a,b]
Bering	0.97	0.17	0.46	0.12	∼ 4500	Buoy data

The wind wave output fields were obtained with time step 3 hours from 1979 to 2019 for the Barents, Kara, Bering, Okhotsk, and EJS and from 1979 to 2020 for the Black and Caspian Seas. We considered SWH (m) as $\left(4\sqrt{m_0}\right)$, where m_0 is the zero-order moment of the wave spectrum. SWH is somewhat of the mean value of 1/3 of the highest waves. The analyzed statistical parameters are the 95% percentile SWH, long-term maximum and mean SWH. Maximum SWH is the highest SWH for the whole modeled period for each
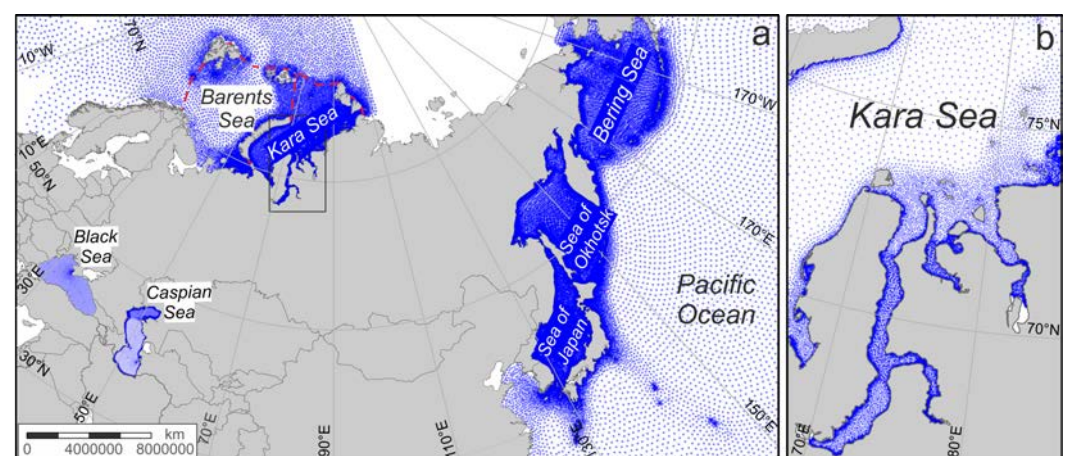
Figure 1. The computational grids for all researched seas (a), the Kara sea and the Gulf of Ob (b). Dashed red lines show the boundaries of the Barents and Kara Seas.

point. If the sea surface was ice covered, the SWH in this node was equal to zero. The mean long-term characteristics include it in calculations as zero data.

2.4. Number of storms recurrence

The storm activity analysis was conducted according to the peak-over-threshold (POT) approach, which is widely used [*Amarouche et al.*, 2020, *Leo et al.*, 2020]. The POT method finds extreme values for some samples that exceed a certain threshold value. Previously we used this approach for the Black, Caspian, Kara and Bering Seas [*Ivanov et al.*, 2022, *Myslenkov et al.*, 2018a, 2021b]. The number of storms with different SWH thresholds from 2 to 8 meters was calculated for each month, each year and each sea. For example, if at least in any one point of the computational grid the SWH exceeded 3 m, then this event would be identified as a storm case with SWH threshold 3 m (Figure 2) in the investigated sea. This event would go on until the SWH would be less than the threshold for all grid points in the basin. Furthermore, when the SWH threshold was exceeded in any one point again, this event would be considered as a next storm event. A period of 9 hours was the minimum interval to distinguish two separate storms that go one by one. The inaccuracy of this method can be caused by storms passing consequently one after another and also when two storms come from different directions at the same time. However, such cases are rare. The proposed algorithm works correctly and it was validated by a visual analysis carried out for several seas. Such spatio-temporal method of storm research allows to take into account all storm events in the entire water area of a selected sea.

We did not consider the threshold of 2–4 m for the Barents and Bering Seas because mean SWH is high there. Therefore, we only analyzed higher thresholds, starting from 4 and up to 8 m. As the result, there are more storms with a threshold of 5 m than any less severe storms with a threshold of 4 m. That means that the SWH did not fall below 4 m for a long time. As 5 m storms are shorter than lower 4 m storms, the number of 5 m storms could have been bigger than the number of 4 m storms.

The number of storms was calculated for the whole area of each sea. To define, for example, sea boundaries for the marginal Barents and Kara Seas, we considered official boundaries from International Hydrographic Organization. They are highlighted in Figure 1 by dashed red lines. Sea limits are restricted to natural geographical features for the other seas, such as narrow straits etc. The boundaries follow the Korean and Tatar Straits for the EJS.
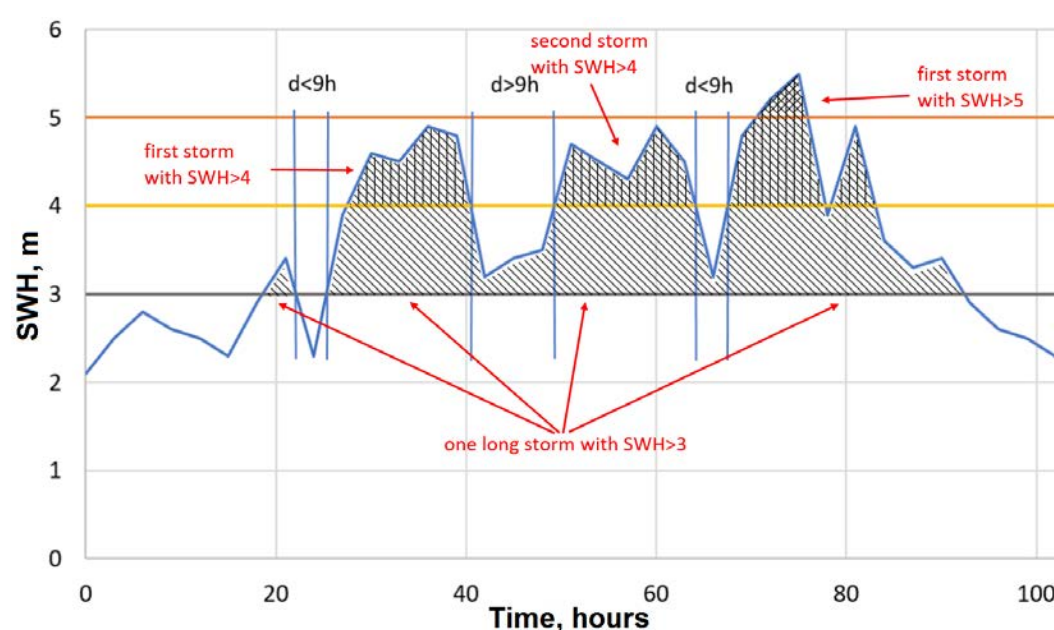

Figure 2. Visual representation of the POT method for storm analysis.

The each of storms, which calculated according to POT approach, has its own duration. We calculated number of stormy days as a sum of each storm duration for the different thresholds for the month or year. The number of stormy days in common with a number of storms allow you to effectively analyze storm activity.

We also use calculated the 95% percentile wind speed (P95 wind) for one point in the center of the each sea. Of course, one point is not responsible for storms in the whole sea, however, as it turned out, the P95 wind has a very high correlation with the number of stormy days. This made it possible to identify a possible reasons for changes in storm activity.

Also we used monthly average Sea ice are data from NOAA (https://www.ncei.noaa.gov/access/monitoring/regional-sea-ice/).

2.5. Indices of Atmospheric Circulation

We analyzed the interannual variability connection between the storm recurrence and seven most popular indices of the atmospheric circulation. We used annual and seasonal January–March (JFM), April–June (AMJ), July–September (JAS) and October–December (OND) periods for mean index values.

The NAO index is based on the surface sea-level pressure difference between the Subtropical (Azores) High and the Subpolar Low (https://www.cpc.ncep.noaa.gov/products/precip/CWlink/pna/nao.shtml). The AO is a large scale mode of climate variability, also referred to as the Northern Hemisphere annular mode (https://www.cpc.ncep.noaa.gov/products/precip/CWlink/daily_ao_index/ao.shtml). The AO is a climate pattern characterized by winds circulating counterclockwise around the Arctic at around 55°N latitude. The positive North Atlantic Oscillation (NAO) and Arctic Oscillation (AO) phases are associated with a poleward shift of cyclone trajectories. It leads to wetter and warmer weather over Northern Europe and, consequently, can influence the number of storms in the Barents and Kara Seas. The influence of the NAO index on the wind sea and swell regional climates in the North and Barents Seas shown in [*Bertin et al.*, 2013, *Semedo et al.*, 2014, *Shimura et al.*, 2013].

PDO (https://www.ncdc.noaa.gov/teleconnections/pdo/) is a recurring pattern of ocean-atmosphere climate variability centered over the middle Pacific latitudes. The PDO is determined by warm or cold surface water in the Pacific Ocean north of 20°N. During the "warm" or "positive" phase the western Pacific becomes cooler, while the eastern part – warmer. During the "cool" or "negative" phase the opposite pattern occurs [*Mantua et al.*, 1997].

The North Pacific Index (NP) is the area-weighted sea level pressure over the region 30°N–65°N, 160°E–140°W [*Trenberth and Hurrell*, 1994]. The NP index is defined to measure interannual to decadal variations in the atmospheric circulation. The NP may have greater impact on wave climate variability in the North Pacific [*Shimura et al.*, 2013].

The El Niño/Southern Oscillation (ENSO) (https://psl.noaa.gov/enso/mei/) a naturally occurring anomalous state of tropical Pacific coupled ocean-atmosphere conditions. The NINO 3.4 (https://psl.noaa.gov/gcos_wgsp/Timeseries/Nino34/) index is one of several El Niño indicators based on sea surface temperature. NINO 3.4 is the average sea surface temperature anomaly in the region bounded by 5°N to 5°S, from 170°W to 120°W. The ENSO, and NINO 3.4 could influence the number of storms in the North Pacific [*Bromirski et al.*, 2013]. El Niño oscillation is mainly considered in the context of water temperature anomalies [*Osipov and Gushchina*, 2021], however, this process also affects the change in global atmospheric circulation. The influence of the ENSO on tropical cyclone intensity in the western Pacific is described by *Camargo and Sobel* [2005]. [*Maslova et al.*, 2020] showed the connection between cyclonic activity in the Black Sea and ENSO index.

North Caspian Index (NCP) is calculated from the normalized 500 hPa pressure difference between averages of North Sea (0°E, 55°N and 10°E, 55°N) and North Caspian (50°E, 45°N and 60°E, 45°N) centers of action. NCP was taken from [*Türkeş and Erlat*, 2018]. NCP presumably influences the cyclones in the Caspian and Black Seas.

We used mean annual and seasonal index values in the correlation analysis with the number of storms for each sea. For visual comparisons, we choose the indices, which show the bigger correlation with a number of storms. In the correlation analysis, all indices were used.

2.6. Trend and Correlation Analysis

The trend quality assessment (linear regression model) was determined by two approaches: by checking the regression coefficients for significance and the adequacy of the regression model. Checking the regression coefficients for significance was carried out on the basis of testing hypotheses that regression coefficients are insignificant (H_0) and significant (H_1):

$$H_0 : a = 0; H_0 : b = 0,$$

$$H_1 : a \neq 0; H_0 : b \neq 0,$$

where a is the dependent regression coefficient and b is the independent regression coefficient. Student t-test (t^*) was calculated for verification using the standard procedure in the Matlab package;

$$t_a^* = \frac{|a|}{\sigma_a}, \quad t_b^* = \frac{|b|}{\sigma_b},$$

$$\sigma_a = \frac{\sigma_y \cdot \left(1 - R^2\right)}{\sigma_x \cdot \sqrt{N-1}}, \quad \sigma_b = \frac{\sigma_y \cdot \sqrt{1 - R^2}}{\sqrt{N-1}}.$$

σ_a and σ_b are standard random calculation errors of the coefficients a and b, R is the correlation coefficient, σ_x and σ_y are standard deviations of the insignificant and significant variables accordingly. The critical value $t_{cr}(\alpha, \nu)$ was determined by the significance level (taken as 10%) and the number of degrees of freedom $\nu = N - 1$, where N is the length of the series. In our case, the length of the series for all seas was 41, except for the Black and Caspian Seas – for them the length of the series was 42. If $t^* > t_{cr}$ H_0 was rejected, the corresponding regression coefficient was significant. If $t^* < t_{cr}$, then there was no reason to reject H_0, so the corresponding regression coefficient was insignificant.

The adequacy of the regression model was assessed by the F-test (based on the Student's t-test). We put forward H_0 for the equality of the variances

$$H_0 : \sigma_y = \sigma_e : H_1 : \sigma_y^2 \neq \sigma_e^2,$$

(the variance of the model is σ_y^2 and the variance of the residuals is σ_e^2). For verification, Fisher's criterion (F^*) was used;

$$F^* = \frac{\sigma_y^2}{\sigma_e^2},$$

It was compared with F_{cr} with a given significance level ($\alpha = 0.10$) and the number of degrees of freedom $n_1 = N_1 - 1$ and $n_2 = N_2 - 1$. If $F^* > F_{cr}$, then was rejected, which means the adequacy of the regression model in this case.

3. Results and Discussion

3.1. Quality Assessment of the Wind Wave Model

A comparison of the modeled and measured SWH for the buoy station in the Bering Sea is shown in Figure 3. We used the wind data from ERA5 and CFSv2 reanalysis for the wave model run. Both model versions provide the wave height and phase of the individual storm event quite well, but there is some errors for the SWH ≥ 7 m.

Statistical results based on wave measurements from 1 January 2018 to 31 December 2019. The correlation coefficient R is 0.969, the Bias is 0.17 m, and the RMSE is 0.46 m for this series based on CFSv2 wind. For the model version based on ERA5 wind, the R is 0.973, the Bias is -0.25 m, and the RMSE is 0.52 m. Obviously, both versions of the model give almost the same result, but we chose CFSv2 because the RMSE is slightly less.
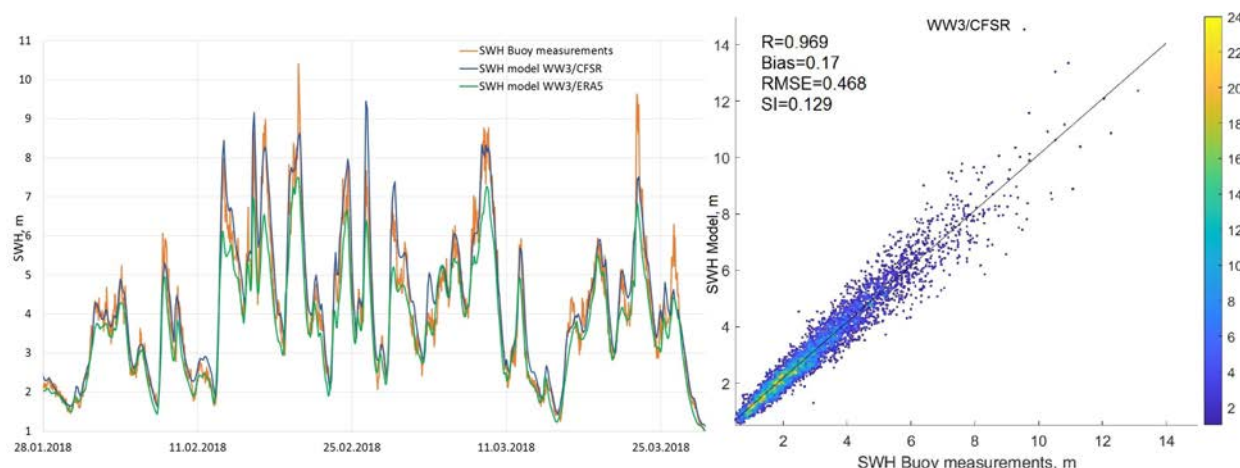
Figure 3. Time series comparison (left panel) for the period from 28 January 2018 to 28 March 2018 and scatter diagram (right panel) of the measured and simulated SWH for buoy station No 46035 in the Bering Sea for the period from 1 January 2018 to 31 December 2019 (4583 samples).

Such simulation of quality corresponds to the world class of modern wave model realizations [*Stopa et al.*, 2016, *Van Vledder and Akpınar*, 2015]. It allows to estimate the regular and extreme characteristics of the wave climate, as well as the interannual variability of storm activity. The main goal of the study was to evaluate long-term trends and find correlations of storms with atmospheric indices. If we use different datasets that will give us a slightly different RMSE error in SWH: 0.3 or 0.5 m. But it does not affect the trends and interannual storms variability.

Some statistical data are presented in Table 1 for the studied seas. According to this table, the highest *R* was obtained for the Bering and Caspian Seas. The lowest *R* was obtained for the Black Sea. There is a 0.12 Scatter index (SI) in the Bering Sea and 0.36–0.65 SI in the Black Sea. It shows that the model gives adequate results for the considered seas.

3.2. The Mean and Extreme Wave Conditions
The Barents Sea

The considered sea boundaries for the Barents Sea are marked by dashed green lines (Figure 4). The mean long-term SWH is 0.5–1 m in the northern and northeastern parts of the sea (Figure 4) due to the presence of ice. The mean SWH is about 1.5–2 m in the central Barents and neighboring it the western part of the Norwegian Sea. The highest mean SWH is approximately 2.3 m. It was found near the border with the Norwegian Sea. The 95% percentile SWH is about 3–5 m in the central and western parts of the Barents
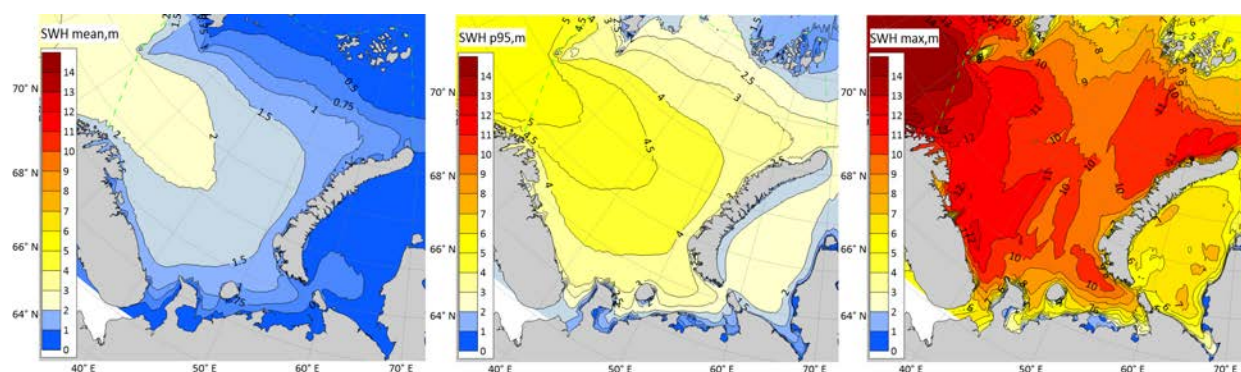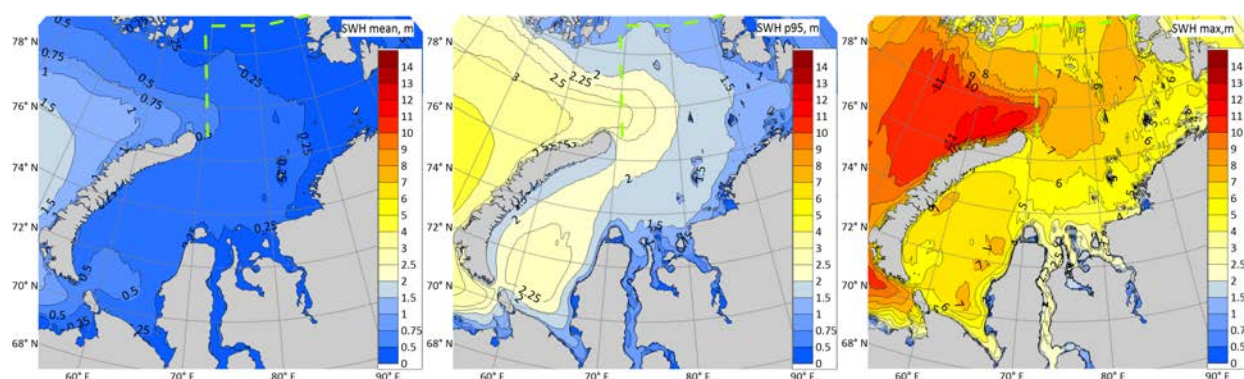

Figure 4. The modeled long-term mean, 95% percentile, and maximum SWH in the Barents Sea (1979–2019). Dashed green lines marked sea boundaries.

Sea. The maximum SWH was more than 13 m in the west part of the sea. The maximum SWH for the 41-year time period reaches 7–8 m on the north boundary of the Barents Sea. It is remarkable that there is an area of maximum SWH with values of 10–11 m, right on the border with the Kara Sea in the north-east.

The Kara Sea

The mean long-term (from 1979 to 2019) SWH is about ≤ 0.5 m in the Kara Sea (Figure 5). The highest mean SWH is about 0.6 m and is found in the area of the Kara Strait. The 95% percentile SWH is about 1–2 m in the Kara Sea. The wave conditions of the Kara Sea are under the influence of the Barents Sea wind wave in the west and ice fields in the northern part. The long-term maximum SWH for the most part of the sea is about 5–7.5 m. The highest maximum SWH is about 10.6 m and is found north of Novaya Zemlya islands, at the border with the Barents Sea.
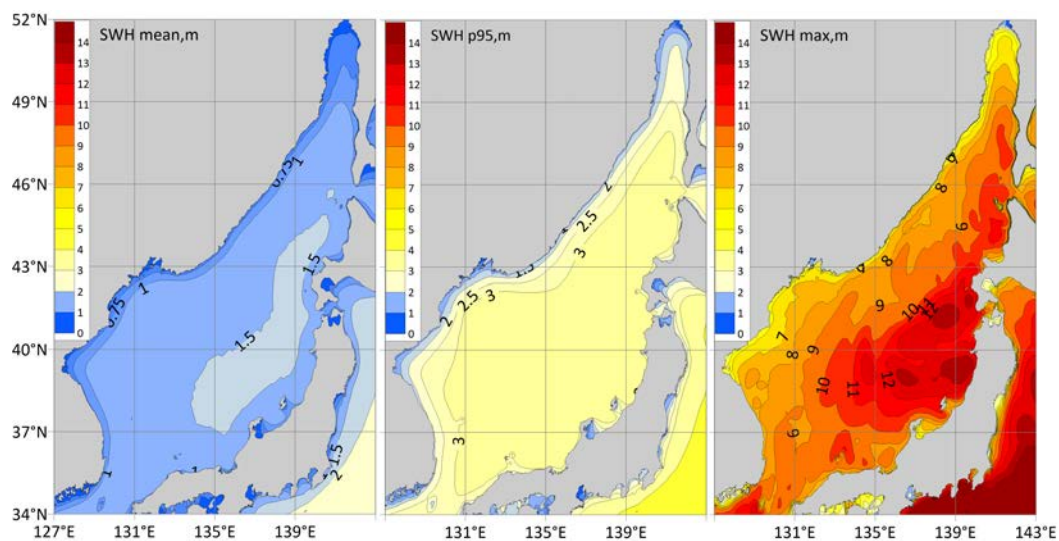

Figure 5. The modeled long-term mean, 95% percentile, and maximum SWH (m) in the Kara Sea (1979–2019). Dashed green lines marked sea boundaries.

The Sea of Japan

The modeled long-term mean SWH in the EJS is 1–1.5 m (Figure 6) in the open part and less than 1 m along the Korean, Russian coasts. The ice fields in the EJS is generally seen only in the Strait of Tatary. The 95% percentile SWH is 3 m in the central part and 1–2 m along the Russian and Korean coast. The maximum SWH varies from 5 to 13 m. The highest wave area is in the eastern part of the sea, near the west coast of the Honshu Island, between 38–42°N. This area is in the way of a typhoon spreading from the south-west [*Mei and Xie*, 2016].

The Sea of Okhotsk

The modeled mean SWH for the Sea of Okhotsk ranges from 1 to 2 m for the most area of the sea (Figure 7). Mean SWH is less than 1 m around the Sakhalin Island. That is also true for the whole Russian coast from 53°N to the Kamchatka Peninsula. Mean SWH varies from 1 to 2 m at the east Kamchatka coast. Its maximum is about 2 m, it is the same for the area near the Kuril Islands. The wave energy comes from the North Pacific. The 95% percentile SWH is lower than 2 m in the Sakhalin Gulf. Northward 95% percentile SWH varies from 1 to 2 m along the coast toward the Shelikhov Gulf. On the west Kamchatka coast, it ranges from 2 to 3 m. In the central part 95% percentile SWH varies from 3 to 5 m, Near 48°N it exceeds 5 m. The maximum SWH space distribution has four local rises: two main in the central part of the Okhotsk Sea with a maximum of 14 m. Others two local zones with 12–13 m maximum is located near Shantar Islands near 140°E. The long-term SWH maximum is 16.5 m.

Figure 6. The modeled long-term mean, 95% percentile, and maximum SWH in the EJS (1979–2019).
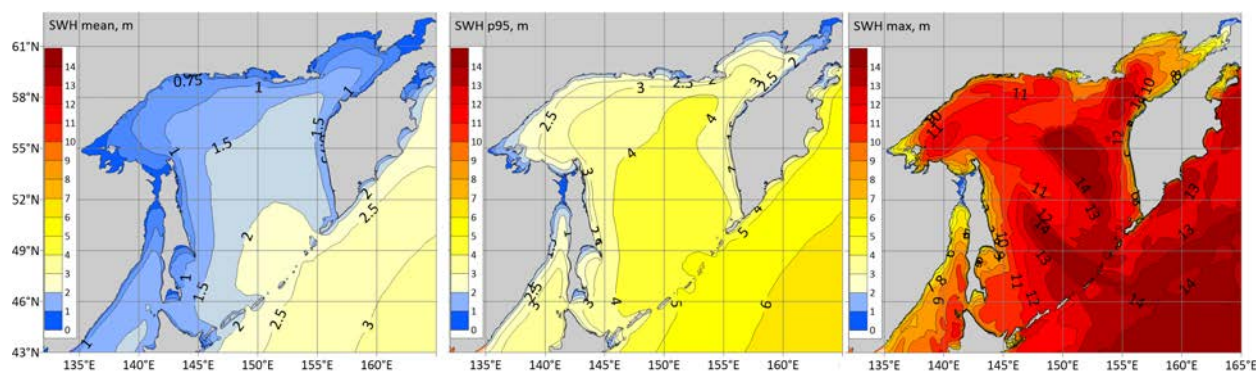
Figure 7. The modeled long-term mean, 95% percentile, and maximum SWH in the Sea of Okhotsk (1979–2019).
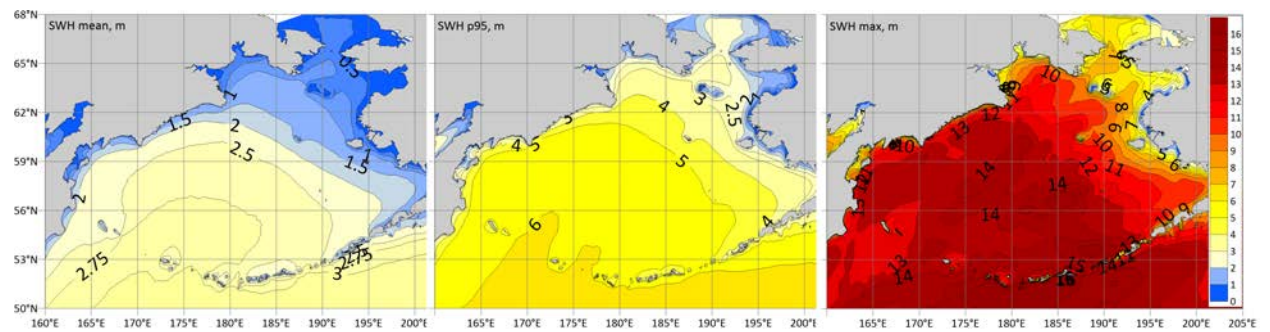
The Bering Sea

The long-term mean SWH for 41-year period in the Bering Sea changes from 0.5 to 2.9 m (Figure 8). Waves pass with maximum SWH 14–15 m through the Aleutian Ridge. The long-term SWH maximum is 16.5 m. The 95% percentile SWH here exceeds 6 m. The 95% percentile is from 6 to 5 m in the central part. Its value decreases on its way towards the Bering Strait. According to the obtained hindcast, the maximum SWH on the Russian coast is about 12–13 m. It decreases to 5–8 m in the Gulf of Anadyr. Wind waves are weaker near the Alaska coast compared with the west part of the Bering Sea, because the Alaska Peninsula does not let absolute propagation of the wind waves from the North Pacific. Calculated SWH values are minimal on the east Bering Sea coast.

The Black Sea

According to *Arkhipkin et al.* [2014], the average SWH of the Black Sea did not exceed 0.7 m. *Akpınar et al.* [2016], *Gippius and Myslenkov* [2020] have calculated that SWH did not exceed 1.1 m in the southwestern part of the Black Sea. The long-term mean SWH for 42-year period in the most part of Black Sea is less than 1 m (Figure 9). The 95% percentile SWH is 2.5 m in the western part. The maximum calculated SWH for the whole period was 9 meters and it did not coincide with the 95% percentile SWH distribution. This zone located in the east part of the Black Sea, near 44°N and the city of Sochi. The highest waves of 8 m were also observed near the south-western Crimea coast.

Figure 8. The modeled long-term mean, 95% percentile, and maximum SWH in the Bering Sea (1979–2019).
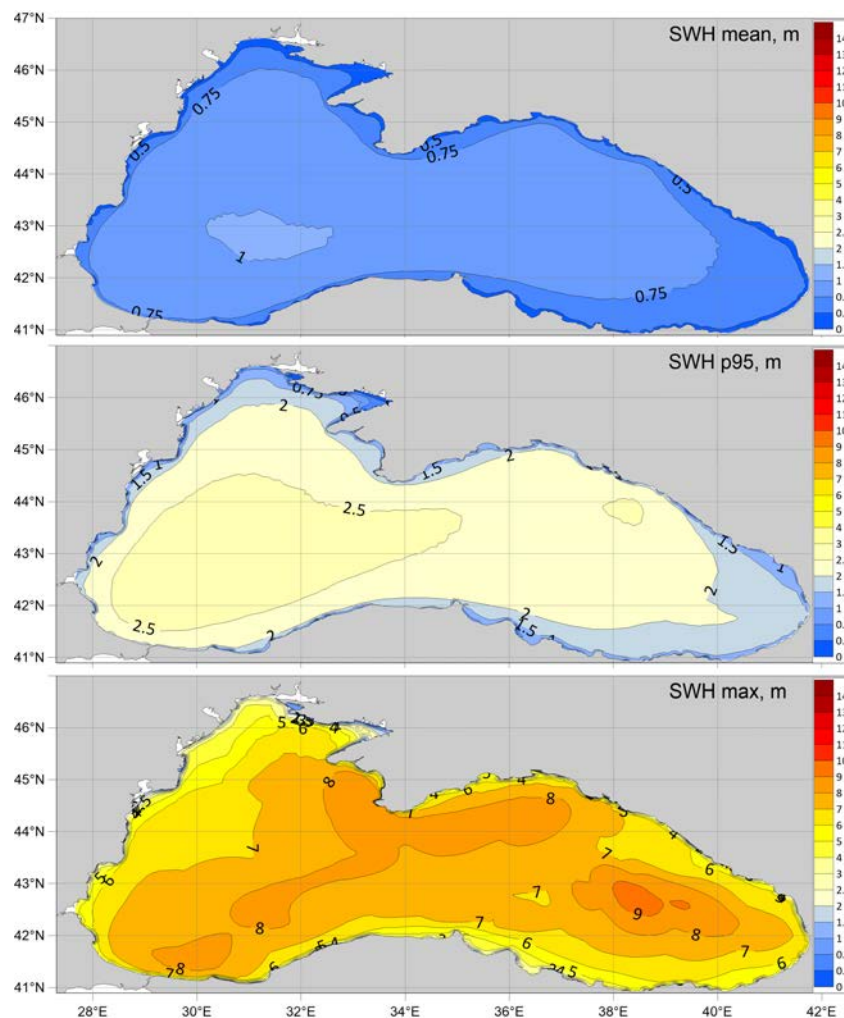
Figure 9. The modeled mean SWH, 95% percentile SWH, and maximum SWH in the Black Sea (1979–2020).

The Caspian Sea

The mean SWH is about 0.5–1 m in the Caspian Sea (Figure 10). The highest mean SWH is about 1 m in the central part of the sea. In the north, due to the shallow depths and ice fields in winter, the mean SWH did not exceed 0.5 m. The 95% percentile SWH is about 2–2.5 m. The maximum SWH is about 5–8 m in the Caspian Sea. The highest maximum SWH is about 8.2 m. It was found in the central part of the sea.
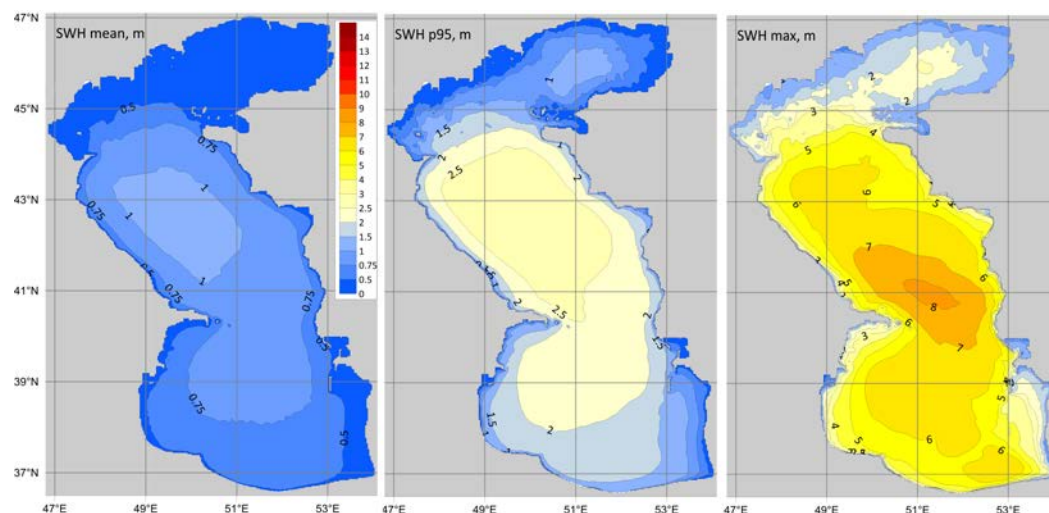
Figure 10. The modeled mean SWH, 95% percentile SWH, and maximum SWH in the Caspian Sea (1979–2020).

3.3. Linear trends of the number of storms and the relations with atmospheric indices

The main statistical parameters for the wave height and the number of storms are shown in Table 2 for all studied seas. The highest mean and maximum SWH are observed in the Bering, Barents Seas and the Sea of Okhotsk. The data highlight the differences of the wave climate and storm activity in studied seas.

Table 2. General statistics of SWH, number of storms and trends for seven Russian Seas

Sea	Mean SWH	P95 SWH	Max SWH	Average number of storms SWH > 6 m per year	Average number of storms SWH > 7 m per year
Barents	1–2	3–4	14	24.6	13.7
Kara	0.5	1.5–2	7.2	1.6	0.5
Black	0.5–1	2–2.5	9.5	1.7	0.4
Caspian	0.5–1	2–2.5	8.3	1.1	0.1
Japan	1–1.5	2–3.5	13.9	16.9	9
Okhotsk	1–2	3–4	15.5	33.4	22.4
Bering	2–2.5	3–5	16.5	48	38

The number of stormy days for the different SWH thresholds are shown in Table 3 for all seven studied seas. The maximum number of stormy days are observed in the Bering Sea. Consequently, in the Bering Sea, the SWH is more than 3 m most of the year. In the Barents Sea and the Sea of Okhotsk the number of stormy days with SWH > 3 m is more 200.

We performed a trend-significant analysis in the number of storms with different thresholds, based on the F-test and t-test (method described in the subsection 2.6). In Table 4, trends analysis presented. Generally, both criteria gave the same result except one case for the Barents Sea.

We found two positive trends for SWH ≥ 3 and 6 m for the EJS. A positive significant trend was calculated for the highest storms with SWH ≥ 8 m in the Sea of Okhotsk and Bering Sea. For the Caspian Sea, two positive trends for SWH ≥ 3 and 4 m were revealed. Positive trends were found for all thresholds except the SWH ≥ 6 m in the Kara Sea. The most intense increase in the number of storms was observed in the Kara Sea: the number of

Table 3. Number of stormy days per year for the different SWH for seven Russian Seas

Sea	SWH > 2 m	SWH > 3 m	SWH > 4 m	SWH > 5 m	SWH > 6 m	SWH > 7 m	SWH > 8 m
Barents	–	215	118	57	26	11	5
Kara	119	39	12	3	1	–	–
Black	123	42	13	3	1	–	–
Caspian	114	36	9	2	–	–	–
Japan	–	147	68	30	13	6	2
Okhotsk	–	218	127	73	39	21	10
Bering	–	283	209	140	89	51	27

storms over 3 m was more than doubled over a 40-year time period. A negative trend in the Bering Sea was identified for storms with SWH ≥ 5 , but we think that it is a consequence of the POT method calculations (in number of stormy days we found the positive trend). Only in the Black Sea negative significant trend was found for storms with SWH ≥ 2 m. As a result, we can say that in the all studied seas (except the Black Sea), storm activity from the 1979 to 2019 is either increasing or neutral, which is confirmed by the global trends of world ocean wind and waves [*Young and Ribal*, 2019].

Table 4. Trend analysis for the number of storms. Green cell – significant and positive trend, blue – significant and negative, «–» means that trend analysis was not conducted

Sea / SWH threshold	2 m		3 m		4 m		5 m		6 m		7 m		8 m	
	F-test	t^*	F-test	t^*	F-test	t^*	F-test		F-test	t^*	F-test	t^*	F-test	t^*
Japan	–	–	Sign	Sign	Insign	Insign	Insign	Insign	Sign	Sign	Insign	Insign	Insign	Insign
Okhotsk	–	–	–	–	–	–	Insign	Insign	Insign	Insign	Insign	Insign	Sign	Sign
Bering	–	–	–	–	–	–	Sign	Sign	Insign	Insign	Insign	Insign	Sign	Sign
Black	Sign	Sign	Insign	Insign	Insign	Insign	Insign	Insign	–	–	–	–	–	–
Caspian	Insign	Insign	Sign	Sign	Sign	Sign	Insign	Insign	–	–	–	–	–	–
Kara	Sign	Sign	Sign	Sign	Sign	Sign	Sign	Sign	Insign	Insign	Sign	Sign	–	–
Barents	–	–	–	–	–	–	Insign	Insign	Insign	Insign	Insign	Insign	Insign	Insign

Correlation analysis of all atmospheric indices and number of storms was done for all thresholds for each sea to study its connection with the global atmospheric circulation. The results of a correlation analysis for annual averages are shown in Table 5. The relation between the interannual variability of the number of storms and indices is rather weak. The positive R was 0.58 between SWH ≥ 8 m in the Bering Sea with the NP index and the negative R −0.44 with the PDO index. In the Black Sea for SWH ≥ 4 m, weak negative R with the NAO index was registered. In the Barents Sea, for SWH ≥ 7–8 m the R 0.51–0.56 with the AO index and with the NCP index is positive. The obtained result can be explained by the fact that most of the analyzed seas are inner or semi-closed, except the Barents and the Bering seas. In semi-enclosed seas, storms are formed due to the local synoptic processes, ice conditions, basin orography, bathymetry and are weakly dependent on a global atmospheric indices. On the other hand, the Barents Sea is completely open to the wave energy from the North Atlantic, and in the Bering Sea there are very wide straits that also allow propagating of the wave energy from the Pacific Ocean.

Table 5. Interannual correlation analysis of number of storms and atmospheric indices for average annual data. *R* values < −0.4 marked as blue and values > 0.4 marked as red

Sea	≥ (m)	Annual Index						
		AO	NAO	NP	ENSO	PDO	NINO 3.4	NCP
Japan	3	0.01	0.02	0.23	−0.22	−0.22	−0.18	−0.02
	4	−0.08	0.03	0.12	0.11	−0.05	0.11	−0.10
	5	−0.12	0.07	0.09	0.03	−0.12	0.13	−0.27
	6	−0.08	0.02	0.04	0.05	−0.10	0.22	−0.17
	7	−0.18	−0.07	0.03	0.16	0.08	0.32	−0.10
	8	−0.23	−0.11	0.01	0.22	0.13	0.35	−0.15
Okhotsk	4	−0.16	0.04	−0.18	0.28	0.36	0.14	0.14
	5	−0.22	−0.04	0.10	0.25	0.14	0.31	−0.12
	6	−0.30	−0.29	0.03	0.18	0.07	0.28	−0.25
	7	−0.20	−0.10	0.19	−0.01	−0.18	0.15	−0.32
	8	−0.10	−0.11	0.21	−0.29	−0.24	−0.14	−0.20
Bering	4	0.12	0.18	−0.03	0.26	0.17	0.17	0.15
	5	−0.03	0.22	−0.14	0.27	0.32	0.14	0.04
	6	0.07	0.20	0.22	−0.06	−0.09	−0.08	0.05
	7	−0.04	0.05	0.32	−0.15	−0.32	−0.11	−0.26
	8	0.27	0.16	0.58	−0.18	−0.44	−0.06	0.06
Black	2	−0.18	−0.20	−0.24	0.13	0.17	0.04	−0.08
	3	−0.30	−0.25	−0.21	−0.01	0.12	0.01	−0.27
	4	−0.35	−0.44	−0.37	−0.07	0.14	−0.07	−0.05
	5	−0.18	−0.21	−0.16	−0.10	0.08	−0.05	−0.28
	6	−0.02	0.04	0.00	−0.23	−0.09	−0.16	−0.25
Caspian	2	−0.06	0.04	0.07	0.14	0.00	0.17	−0.08
	3	0.29	0.24	0.13	0.07	0.05	0.14	0.04
	4	−0.02	−0.10	−0.15	0.26	0.24	0.31	−0.05
	5	−0.25	−0.18	−0.20	0.12	0.11	0.19	−0.17
	6	−0.32	−0.29	−0.27	0.08	0.15	0.10	−0.33
Kara	2	0.17	−0.01	−0.01	−0.12	0.11	−0.09	0.19
	3	0.13	0.08	0.17	−0.16	−0.11	0.00	−0.03
	4	0.06	0.03	0.26	−0.11	−0.13	0.04	−0.21
	5	0.11	0.12	0.31	−0.02	−0.19	0.10	−0.20
	6	0.02	0.01	0.24	−0.14	−0.18	−0.11	−0.38
	7	0.03	0.06	0.17	−0.09	−0.12	−0.03	−0.24
Barents	4	0.10	0.06	0.11	0.04	−0.10	0.12	−0.10
	5	0.39	0.31	0.07	−0.05	−0.21	−0.05	0.20
	6	0.40	0.37	0.04	0.00	−0.10	−0.03	0.37
	7	0.46	0.32	0.27	0.08	−0.03	0.04	0.44
	8	0.51	0.27	0.10	0.28	0.10	0.26	0.56

The same correlation analysis was done for the atmospheric indices and number of stormy days, because the storm duration variability is differ from number of storms. We found only the weak $R \sim 0.55$ for the Bering and Barents Seas (Table 6), which confirms the conclusions made above.

Table 6. Interannual correlation analysis of number of stormy days and atmospheric indices for average annual data. *R* values < −0.4 marked as blue and values > 0.4 marked as red

Sea	≥ (m)	Annual Index						
		AO	NAO	NP	ENSO	PDO	NINO 3.4	NCP
Japan	3	−0.09	0.00	0.09	0.07	−0.13	0.18	−0.11
	4	−0.08	−0.02	0.03	0.07	−0.10	0.22	−0.22
	5	−0.18	−0.04	0.05	0.03	−0.11	0.22	−0.32
	6	−0.22	−0.05	0.04	0.12	0.03	0.32	−0.26
	7	−0.19	−0.02	0.01	0.20	0.14	0.36	−0.23
	8	−0.13	0.03	0.02	0.27	0.14	0.40	−0.21
Okhotsk	4	0.01	−0.13	0.22	−0.29	−0.35	−0.14	−0.22
	5	−0.06	−0.19	0.21	−0.22	−0.33	−0.03	−0.27
	6	−0.07	−0.12	0.14	−0.14	−0.20	0.07	−0.26
	7	−0.04	−0.02	0.19	−0.22	−0.29	−0.03	−0.20
	8	−0.05	−0.04	0.15	−0.17	−0.16	0.01	−0.23
Bering	4	−0.18	−0.30	0.13	−0.02	−0.13	0.03	−0.21
	5	−0.04	−0.01	0.41	−0.19	−0.37	−0.10	−0.23
	6	0.07	−0.01	0.52	−0.18	−0.51	−0.08	−0.16
	7	0.17	0.12	0.55	−0.20	−0.44	−0.12	0.02
	8	0.27	0.16	0.46	−0.08	−0.31	0.01	0.05
Black	2	−0.34	−0.27	−0.42	0.23	0.27	0.16	−0.20
	3	−0.40	−0.41	−0.36	0.04	0.20	−0.01	−0.34
	4	−0.27	−0.29	−0.25	−0.04	0.11	−0.05	−0.26
	5	−0.15	−0.18	−0.16	−0.21	−0.05	−0.21	−0.28
	6	−0.08	0.08	−0.01	−0.20	−0.18	−0.14	−0.30
Caspian	2	0.02	0.01	0.17	−0.03	−0.01	0.02	−0.16
	3	0.09	0.03	0.11	0.01	0.04	0.08	−0.19
	4	−0.27	−0.28	−0.02	0.14	0.12	0.23	−0.37
	5	−0.36	−0.33	−0.16	0.09	0.06	0.18	−0.40
	6	−0.16	−0.12	−0.21	0.17	0.19	0.18	−0.21
Kara	2	0.11	−0.01	0.22	−0.11	−0.18	0.08	0.00
	3	0.05	−0.08	0.31	−0.12	−0.18	0.07	−0.18
	4	0.03	−0.03	0.33	−0.07	−0.16	0.04	−0.23
	5	0.11	0.03	0.27	−0.07	−0.19	0.01	−0.29
	6	0.20	0.13	0.23	−0.08	−0.10	−0.05	−0.21
	7	0.03	0.08	0.21	−0.10	−0.04	−0.09	−0.15
Barents	4	0.29	0.23	−0.09	0.09	0.10	0.09	0.23
	5	0.55	0.37	0.19	0.11	−0.12	0.11	0.43
	6	0.48	0.27	0.17	0.18	0.00	0.16	0.40
	7	0.46	0.18	0.20	0.21	0.08	0.22	0.43
	8	0.38	0.14	0.02	0.33	0.22	0.34	0.45

Storm activity had different intensification during a year, so we conducted an interannual correlation analysis for JFM, AMJ, JAS and OND periods. Such standard approach for season choice was used for all seas. We understand that for each region, time period shift, associated with seasons could lead to the *R* changes. We have conducted several tests for the Barents Sea, where correlation analysis was held with a month shifting. The difference was insignificant and the general patterns did not change. Correlation analysis of all atmospheric indices, number of storms and number of stormy days was done for the different seasons. The main results of analysis for the number of storms are shown in Tables A.1–A.2 (https://doi.org/10.13140/RG.2.2.15401.67688). The weak positive

R between number of storms and its duration SWH ≥ 8 m in the Sea of Okhotsk with NP index was found for the JFM period. A weak negative R with the ENSO and NINO index for the JFM period was revealed in the Sea of Okhotsk. The same situation applies to the Bering Sea, however, positive R of 0.6 between NP index and SWH ≥ 8 m attests to strong connection for the JFM period. The same situation, but with the opposite sign of R was found for SWH ≥ 4 m in the Bering Sea, but it was determined by the POT method. In the Barents Sea for SWH ≥ 5–8 m positive R with AO index and with NCP index registered for different seasons, but a stronger R of 0.54 was in the JAS period. In the Caspian Sea for SWH ≥ 2–3 m, a weak positive R with the NCP index is registered in the JFM and OND periods. In the Kara Sea there were no correlation connections detected for all seasons at all.

The main results of analysis for the number of stormy days are shown in Tables A.3–A.4 (https://doi.org/10.13140/RG.2.2.15401.67688). In general obtained results differ little from the correlation analysis for the number of storms. The positive R 0.52 between number of stormy days for the SWH ≥ 7 m in the Bering Sea and NP index and negative R −0.56 was found for the JFM period. We found the negative R −0.59 between number of stormy days for the SWH ≥ 2 m in the Black Sea and AO index for the JFM period. In the Barents Sea strong connection of storm duration for the SWH ≥ 4 and AO index was found for the JFM and OND periods. The weak negative R between stormy days in the Sea of Okhotsk with ENSO and NINO indices was found for the JFM period. The weak positive R between stormy days in the Japan Sea with ENSO and NINO indices was found for the JAS period.

In general, correlation analysis for the different seasons confirmed that stable connections between atmospheric indices observed only for the Barents and Bering Seas. The only difference seasonal analysis from the annual it is a connection between number of stormy days and AO index in the Black Sea for the JFM period.

### 3.4. The number of storms interannual variability

After trend and correlation analyses, annual changes of atmospheric indices, annual changes of the number of storms and its duration for different thresholds and their linear trends were analyzed for each sea separately for a more detailed analysis. We used yearly variation of the Sea ice area, P95 wind (for one point in the center of the sea) to visualize the reasons of changes in storm activity. The choice of indices is due to the best connection which was presented in correlation analysis in subsection 3.3.
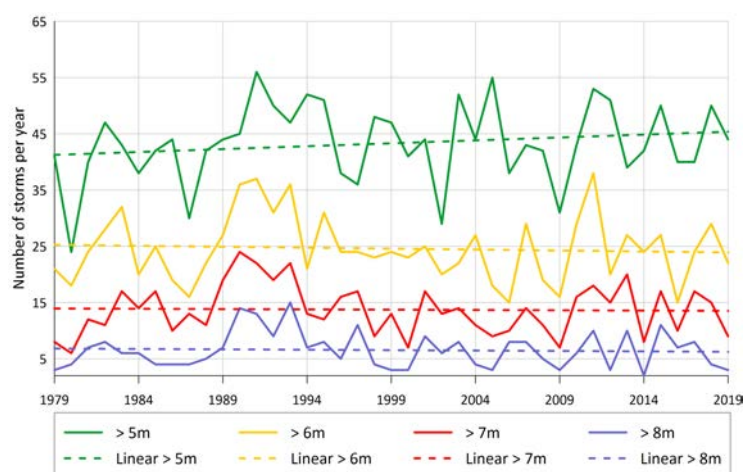
Figure 11. The number of storms for the different thresholds in the Barents Sea.

The Barents Sea

For 41 years, the number of storms with SWH ≥ 5 m was approximately 43 per year, (Figure 11). Wind wave conditions were quite more severe in the Barents Sea, comparing
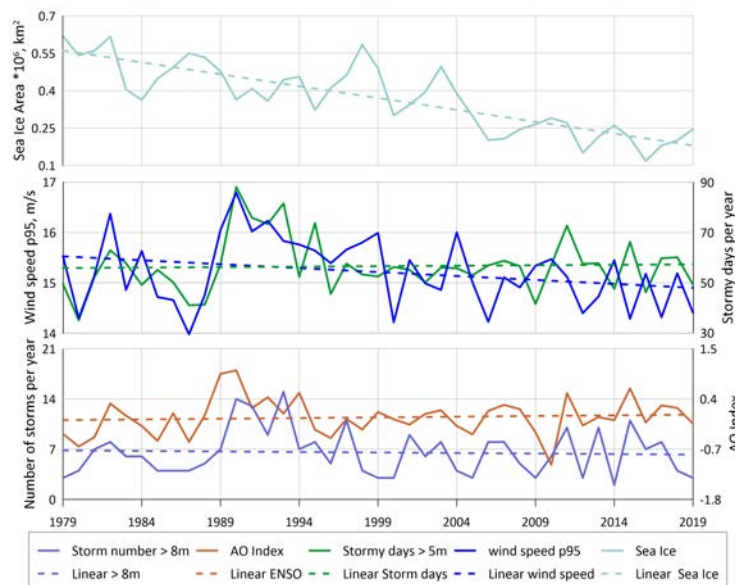
Figure 12. The Sea ice area, AO index, P95 wind, number of stormy days and number of storms in the Barents Sea.

to other considered Russian seas. The storms with SWH ≥ 5 m had local increases in 1991, 2005 and 2011. For the SWH ≥ 6–7 m the local increases were observed in 1990–1993 and in 2011–2013. There was a positive insignificant trend in the Barents Sea for SWH ≥ 5 m and negative insignificant trend for SWH ≥ 6–7 m. However, we can distinguish two rise periods in 1990–1993 and in 2011–2013.

Changes in storm activity are associated with wind variability as shown in Figure 12. Visually, there is a high correlation between the number of stormy days with SWH ≥ 5 m and P95 wind, but the *R* is about 0.5. The main period of high storm activity in 1990–1993 it fits well to wind speed, but small yearly variability often in the opposite phase since 2004 (Figure 12).

The connection of the number and duration of storms with the AO index (*R* 0.55 in Table 6) is visually confirmed. Local storm maxima are observed during years with positive values of the AO index (1990, 2011, and 2015). The positive AO phases are associated with a poleward shift of cyclone trajectories, leading the cyclones move from the North Atlantic to the Barents Sea, which can explain increase in storm activity.

A reduction in the ice area does not affect storm activity in any way, since storms come from the west and fetch from this side is not limited by ice (Figure 12).

The Kara Sea

We found five significant positive trends for the number of storms in the Kara Sea, with SWH from ≥ 2 m to SWH ≥ 7 m for all levels except storms with SWH ≥ 6 m (they were statistically insignificant). The number of storms with SWH ≥ 2 m was approximately 46 per year and with SWH ≥ 3 m ~32 events (Figure 13). The wave heights in the Kara Sea influenced by sea ice variability. The Novaya Zemlya islands limit the wave energy coming from the Barents Sea. The maximum of storms with SWH ≥ 2 m was observed in 1995 (Figure 13). Storms with SWH ≥ 3 m were recorded 30–60 times per year with local increases in 2016 and 2018. For SWH ≥ 4 m, there is a local maximum in 1995 and 2016. For SWH ≥ 5 m, the maximum was recorded in 2018. For SWH ≥ 2–4 m, there is a local minimum of storms in 1998 and 2002. During the entire period, there were positive trends in the Kara Sea for all considered thresholds. The number of storms with SWH ≥ 2 m were increasing by 3 storms in 10 years, with SWH ≥ 3 m by 7 storms in 10 years, with SWH ≥ 4 m by 3 storms in 10 years, with SWH ≥ 5 m by 1 storm in 10 years.
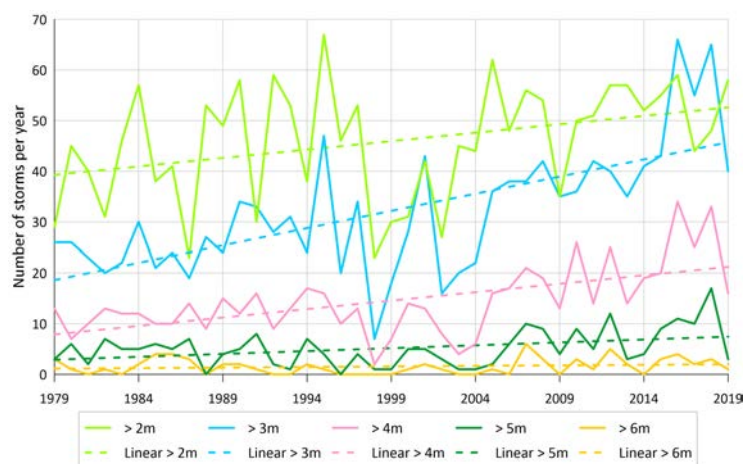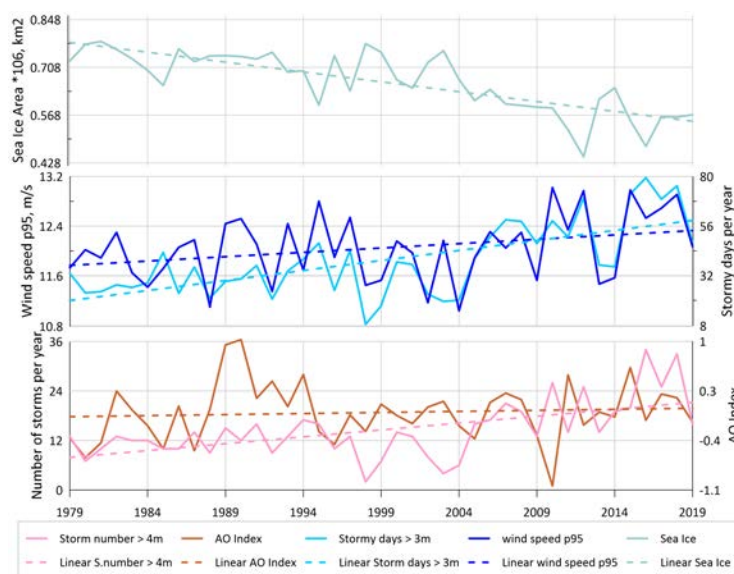
Figure 13. The number of storms for different thresholds in the Kara Sea.

The *R* between P95 wind and the number of storms SWH ≥ 4 m is 0.65. The *R* between P95 wind and the number of stormy days SWH ≥ 3 m is 0.7 (Figure 14). But the wind speed increase insignificantly from 11.8 to 12.3 m/s. Most likely the storm activity in the Kara Sea strongly connected with sea ice area which has halved in recent 41 years. The *R* between sea ice area and the number of storms SWH ≥ 4 m is −0.76 and for the number of stormy days SWH ≥ 3 m is −0.89 (Figure 14).

Visual and correlation analysis shows an absence of connection between any atmospheric indices with the number of storms or storms duration. In contrast to the Barents Sea, storms in the Kara Sea do not arise due to Atlantic cyclones and depends on local ice and wind conditions.

The East/Japan Sea

The positive trends for the number of storms with SWH ≥ 3 m and SWH ≥ 6 m were statistically significant in the EJS. The number of storms with SWH ≥ 3 m was approximately 86 per year, with SWH ≥ 5 m 32 storms (Figure 15). The storms exceeding 8 m were observed on average 4–5 times per year. The local minimum of storms with SWH ≥ 4–7 m was registered in 2001 and 2008. The local maximum of storms with SWH

Figure 14. The Sea ice area, AO index, P95 wind, number of stormy days and number of storms in the Kara Sea.
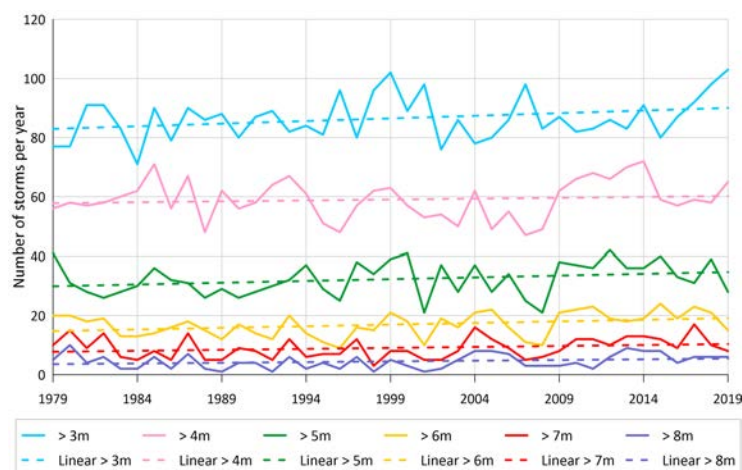
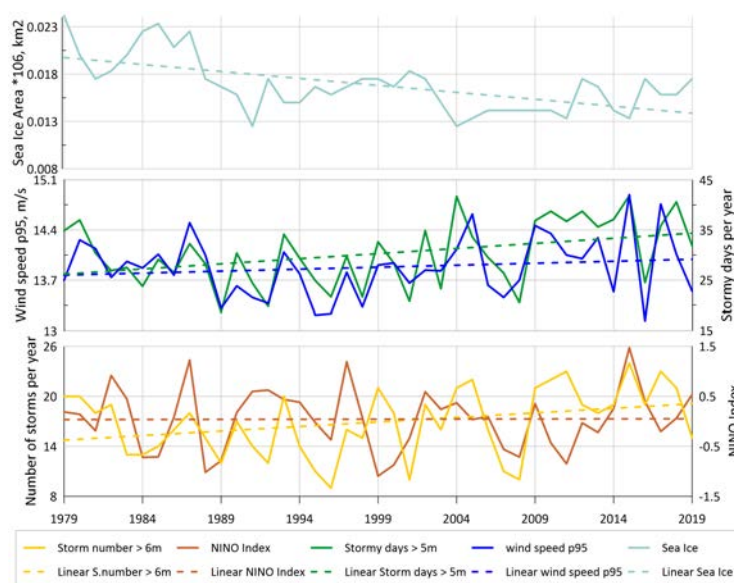**Figure 15.** The number of storms for different thresholds in the EJS.

≥ 6–8 m was registered in 1993, 2004–2005 and 2009–2017. After the period of 2009–2017, a positive trend of the number of storms was found. Over the entire period, there was a positive trend in the EJS for all storm thresholds.

The correlation between P95 wind and the number of storms SWH ≥ 6 m is 0.68. The R between P95 wind and the number of stormy days SWH ≥ 5 m is 0.7 (Figure 16). Sea ice has often a very small area in the EJS Sea and it has no any influence to the storm activity.

A weak positive R between indices NINO and ENSO and the number of stormy days was found only for JAS period (Table A.4 (https://doi.org/10.13140/RG.2.2.15401.67688)) and we didn't see this connections for the yearly data (Figure 16). Thus, the storm activity in the EJS Sea depends only on a local wind conditions.
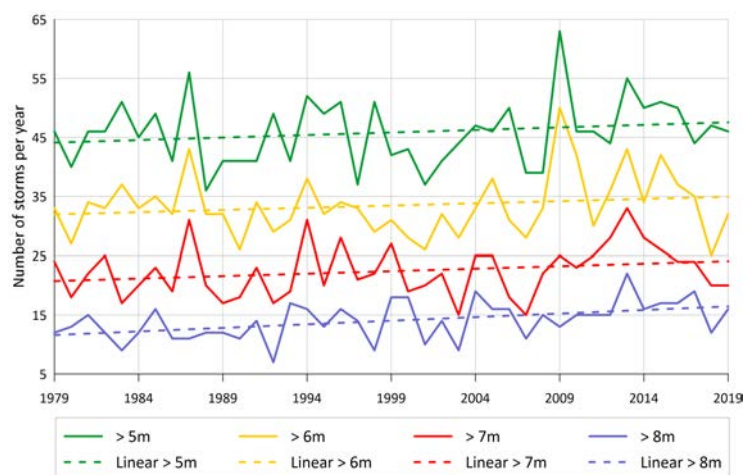
The Sea of Okhotsk

The number of storms with SWH ≥ 4 m was 56 per year in the Okhotsk Sea, with 33 storms exceeding the 6 m criteria (Figure 17). The storms > 8 m were observed on average 12–16 times per year. The local maximum of storms with SWH ≥ 6–7 m was clearly seen in 1987 and 2009. In 2013, the local maximum of storms with SWH ≥ 7–8 m was

Figure 16. The Sea ice area, NINO index, P95 wind, number of stormy days and number of storms in the EJS Sea.
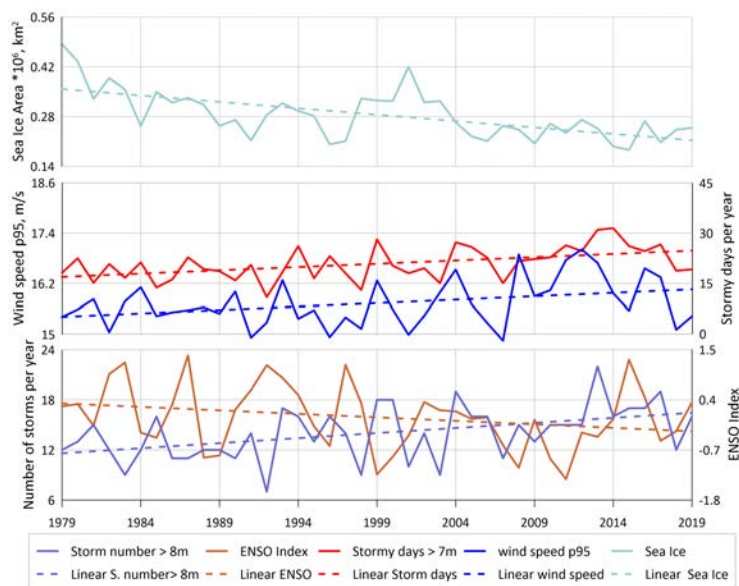
Figure 17. The number of storms for different thresholds in the Sea of Okhotsk.

detected. Over the entire period, there was a positive trend in the Sea of Okhotsk for all storm thresholds and trend for SWH ≥ 8 m was significant.

Visual analysis shows a very weak connections between wind speed and storm activity. The R between P95 wind and the number of storms SWH ≥ 8 m is 0.46. The R between P95 wind and the number of stormy days SWH ≥ 7 m is 0.49 (Figure 18). The R between sea ice area and the number of storms SWH ≥ 6 m is −0.31 and for the number of stormy days SWH ≥ 6 m is −0.47 (Figure 17).

A very weak connections between indices NP, NINO and ENSO and the number of storms and its duration was found only for a January–March period (Tables A.1, A.3 (https://doi.org/10.13140/RG.2.2.15401.67688)).

Taking into account the positive trend in the wind speed and the negative trend in the ice area, we can explain positive significant trend for the number of storms with SWH ≥ 8 m.

Figure 18. The Sea ice area, ENSO index, P95 wind, number of stormy days and number of storms in the Okhotsk Sea.
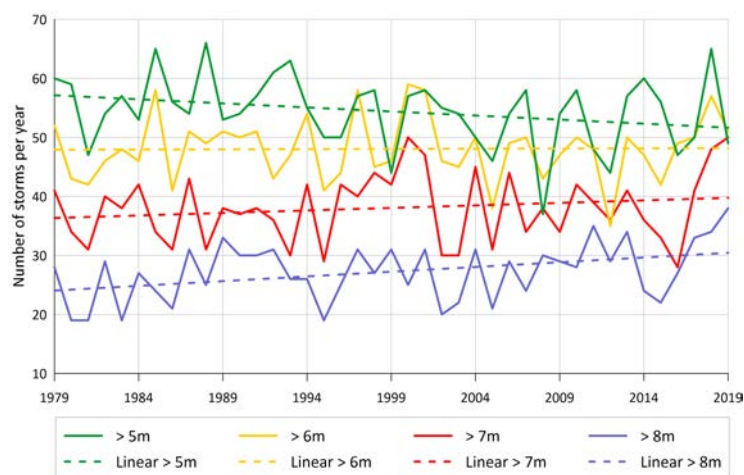
Figure 19. The number of storms for different thresholds in the Bering Sea.

The Bering Sea

The SWH often exceeded 3–4 m (Figure 8) in the Bering Sea, so we considered only the number of storms with SWH ≥ 5–8 m for the analysis. The average number of storms with SWH ≥ 6 m is 48 times per year, with 27 exceeding the 8 m criteria (Figure 19). This is the highest number of 8 m storms between all researched seas. The local maximum of storms with SWH ≥ 7 m is shared by both years 2000 and 2019. The local minimum of storms with SWH ≥ 7–8 m was detected in 1995, 2002 and 2015. A positive significant trend for storms SWH ≥ 8 m found: in the 1979 it was 25 storms per year and more than 30 in 2019. For the entire period in the Bering Sea, there were identified increasing number of storms trends on the Figure 19 for all thresholds, except SWH ≥ 5 m. The decreasing trend for the 5 m storms was significant, but it was caused by the POT method and increasing in the duration of storms. We think that the increase in number of storms and the decrease of the lower height events are the evidence of overall intensification of the storminess in the Bering Sea.

The *R* between P95 wind and the number of storms SWH ≥ 8 m is 0.74. The *R* between P95 wind and the number of stormy days SWH ≥ 7 m is 0.81. Visually, this is well traced and indicates that the wind is the main factor in the variability of storm activity (Figure 20). The *R* between sea ice area and the number of storms SWH ≥ 6 m is −0.2 and it is no any connections between the ice and storm activity.

The positive *R* was found between yearly number of storms and its duration in the Bering Sea with the NP index (Table 5–6). The positive *R* of 0.6 found for the JFM period (Table A.1 (https://doi.org/10.13140/RG.2.2.15401.67688)). Visual analysis confirmed this connections (Figure 20).

The Black Sea

Storms with SWH ≥ 2 m were observed ~75 times per year in the Black Sea. Storms with SWH ≥ 4 m were observed there 17–18 times per year (Figure 21). As for the 6 m threshold, such events occurred there 1–2 times per year on average. The local maximum of storms with SWH ≥ 2 m were clearly visible in 1998. A marked decrease in the number of storms with SWH ≥ 3–4 m occurred between 2017 and 2020 (Figure 21). A negative trend for number of storms SWH ≥ 2 m is clearly visible. Trends for other SWH criteria and in storm duration are neutral.

The correlation between P95 wind and the number of storms SWH ≥ 4 m is 0.65. The *R* between P95 wind and the number of stormy days SWH ≥ 3 m is 0.76 (Figure 22). Since sea ice in the Black Sea appears extremely rarely, it is natural that the main factor for the variability of storm activity is wind.

In the Black Sea for SWH ≥ 4 m, weak negative *R* with the NAO index was registered and confirmed by visual analysis (Figure 22). This connection may be caused by a change
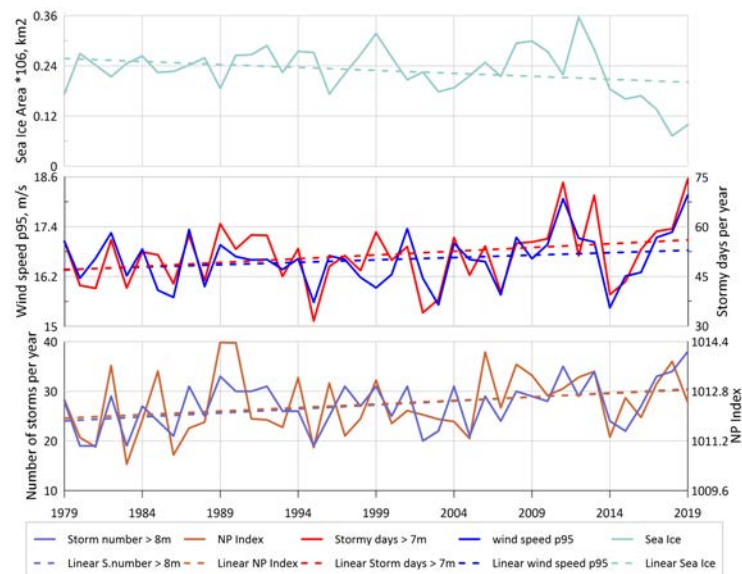
Figure 20. The Sea ice area, NP index, P95 wind, number of stormy days and number of storms in the Bering Sea.
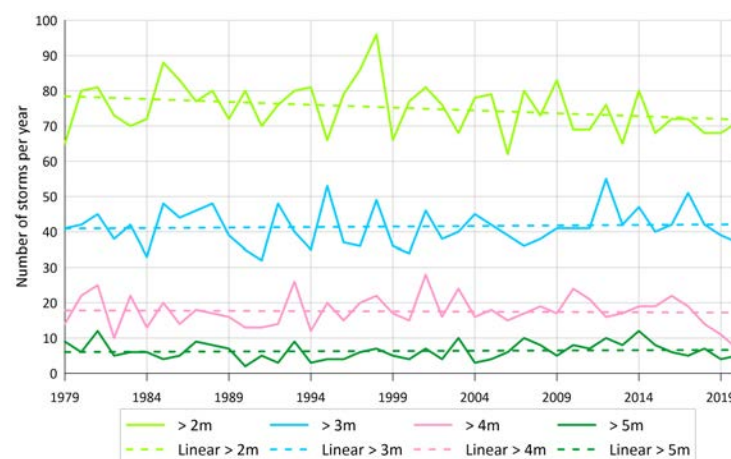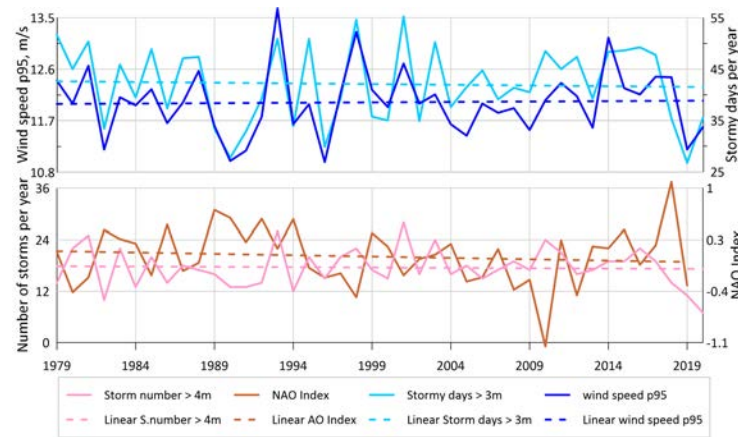

Figure 21. The number of storms for different thresholds in the Black Sea.

in the trajectories of Atlantic cyclones. A negative trend for number of storms SWH ≥ 2 m is not confirmed by wind speed but we see a weak negative trend in the NAO index.

The Caspian Sea

The number of storms with SWH ≥ 2 m was about 90 storms per year in the Caspian Sea (Figure 23). It is greater than in the Black Sea, where only 75 storms per year occurred. The maximum of number storms with SWH ≥ 2 m was observed in 1985. Storms with SWH ≥ 3 m were recorded 30–60 times per year with local increases in 2013–2016. For SWH ≥ 4 m, there was a local maximum of storms in 1998 and 2014. For SWH ≥ 5 m, the maximum was identified in 1979–1983 and 2013. During the entire period, there was a positive trend in the Caspian Sea for storms with SWH ≥ 3 m and SWH ≥ 4 m. The number of storms with SWH ≥ 4 m increased by 2 storms in 10 years, and with SWH ≥ 5 m by 1 storm in 10 years.

The correlation between P95 wind and the number of storms SWH ≥ 4 m is 0.68. The *R* between P95 wind and the number of stormy days SWH ≥ 3 m is 0.83 (Figure 24). Since sea ice in the Caspian Sea appears only in the shallow north part of the sea, it has no influence to storm activity of whole sea.
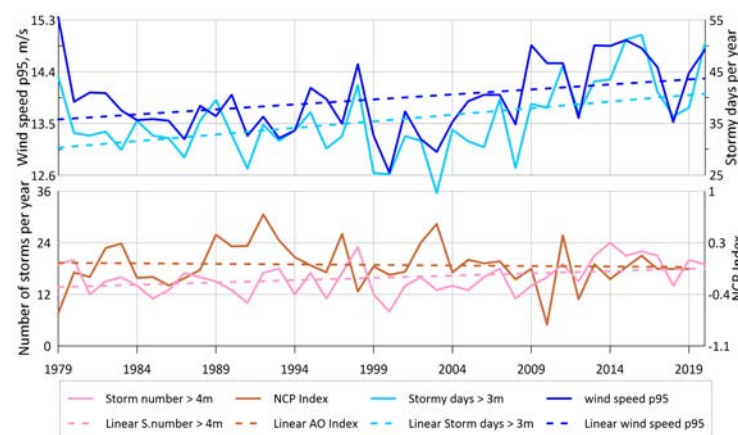
Figure 22. The Sea ice area, NAO index, P95 wind, number of stormy days and number of storms in the Black Sea.
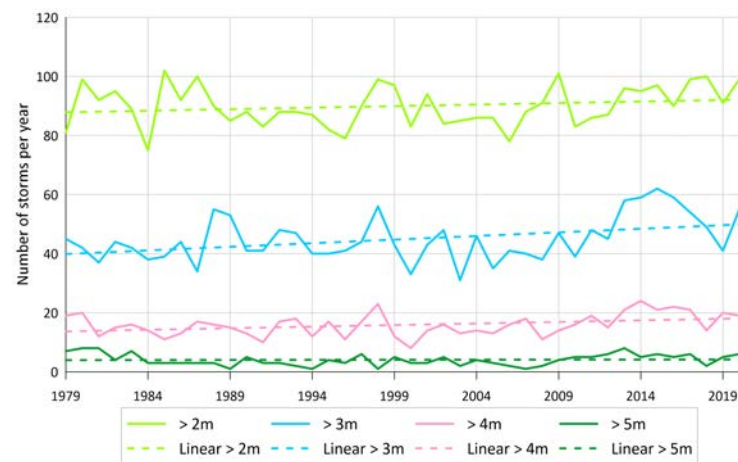
Figure 23. The number of storms for different thresholds in the Caspian Sea.

A very weak positive *R* 0.42–0.45 between number of storms and the NCP index is registered only for the JFM and OND periods (Tables A.1–A.2 (https://doi.org/10.131 40/RG.2.2.15401.67688)). Visual analysis shows an absence of correlation for the yearly number of storms.

Figure 24. The Sea ice area, NCP index, P95 wind, number of stormy days and number of storms in the Caspian Sea.

4. Conclusions

This article presents brand new information about wave climate and storm recurrence in the seven Russian Seas based on the results of wave modeling. The long-term mean SWH, the 95% percentile, and maximum SWH fields were obtained for the time period from 1979 to 2019–2020. The maximum SWH is 15.5 m were in the Sea of Okhotsk and 16.5 m were in the Bering Sea.

A positive significant trend was found for SWH $\geq$ 3 and 6 m for the EJS. Positive significant trends were also registered for SWH $\geq$ 8 m for the Bering Sea and the Sea of Okhotsk. For the Black Sea, a negative significant trend was found for SWH $\geq$ 2 m. Positive significant trends for SWH $\geq$ 3 m and 4 m were registered for the Caspian Sea. In the Kara Sea, positive significant trends for all thresholds except the SWH $\geq$ 6 m were found.

In the all studied seas (except the Black Sea), storm activity from the 1979 to 2019 is either increasing or neutral.

The connection between the interannual variability of number of storms and the indices was very weak. The positive R 0.58 was found between SWH $\geq$ 8 m with the NP index and the negative R equal to -0.44 with the PDO index in the Bering Sea. In the Black Sea for SWH $\geq$ 4 m, the very weak negative R with the NAO index was registered. In the Barents Sea, for SWH $\geq$ 7–8 m a positive R with the AO index. It is worth mentioning that no connection was found between storm activity and atmospheric indices for other seas whatsoever.

The seasonal analysis showed strong positive R 0.6 between NP index and SWH $\geq$ 8 m in the Bering Sea for the JFM period. In the Barents Sea for SWH $\geq$ 5–8 m positive correlation with AO index registered for different seasons, but a stronger R 0.54 was in the JAS period. In the Caspian Sea for SWH $\geq$ 2–3 m, a weak positive R with the NCP index is registered in the JFM and OND periods. The results of analysis for the number of stormy days in general differ little from the correlation analysis for the number of storms. The positive R 0.52 between number of stormy days for the SWH $\geq$ 7 m in the Bering Sea and NP index and negative R -0.56 with PDO index was found for the JFM period. The negative R -0.59 between stormy days for the SWH $\geq$ 2 m in the Black Sea and AO index for the JFM period found. The weak negative R between stormy days in the Sea of Okhotsk with ENSO and NINO indices was found for the JFM period. The weak positive R between stormy days in the Japan Sea with ENSO and NINO indices was found for the JAS period.

In general, correlation analysis for the different seasons confirmed that stable connections between atmospheric indices observed only for the Barents and Bering Seas. The only one difference seasonal analysis from the annual it is a connection between number of stormy days and AO index in the Black Sea for the JFM period.

It was found that the variability of the number storms are weakly related to the global atmospheric indices except the Barents and Bering Seas, which are "open" for the wave energy distribution from the ocean. Storm activity in the inner and semi-closed seas is regulated by the local winds, basin orography and bathymetry (and ice fields in case of Okhotsk and Kara seas) and is very weakly related to global atmospheric indices. These results are fundamental for the wave climate studies.

References

Aarnes, O. J., M. Reistad, Ø. Breivik, E. Bitner-Gregersen, L. I. Eide, O. Gramstad, A. K. Magnusson, B. Natvig, and E. Vanem (2017), Projected changes in significant wave height

toward the end of the 21st century: Northeast Atlantic, *Journal of Geophysical Research: Oceans*, *122*(4), 3394–3403, https://doi.org/10.1002/2016jc012521.

Akpınar, A., B. Bingölbali, and G. P. Van Vledder (2016), Wind and wave characteristics in the Black Sea based on the SWAN wave model forced with the CFSR winds, *Ocean Engineering*, *126*, 276–298, https://doi.org/10.1016/j.oceaneng.2016.09.026.

Akpınar, A., H. Jafali, and E. Rusu (2019), Temporal variation of the wave energy flux in hotspot areas of the Black Sea, *Sustainability*, *11*(3), 562, https://doi.org/10.3390/su11030562.

Amarouche, K., and A. Akpınar (2021), Increasing trend on storm wave intensity in the western Mediterranean, *Climate*, *9*(1), 11, https://doi.org/10.3390/cli9010011.

Amarouche, K., A. Akpınar, N. E. I. Bachari, and F. Houma (2020), Wave energy resource assessment along the Algerian coast based on 39-year wave hindcast, *Renewable Energy*, *153*, 840–860, https://doi.org/10.1016/j.renene.2020.02.040.

Amarouche, K., A. Akpınar, and A. Semedo (2022), Wave storm events in the Western Mediterranean Sea over four decades, *Ocean Modelling*, *170*, 101,933, https://doi.org/10.1016/j.ocemod.2021.101933.

Amini, E., R. Asadi, D. Golbaz, M. Nasiri, S. T. O. Naeeni, M. M. Nezhad, G. Piras, and M. Neshat (2021), Comparative study of oscillating surge wave energy converter performance: a case study for southern coasts of the Caspian Sea, *Sustainability*, *13*(19), 10,932, https://doi.org/10.3390/su131910932.

Amirinia, G., B. Kamranzad, and S. Mafi (2017), Wind and wave energy potential in southern Caspian Sea using uncertainty analysis, *Energy*, *120*, 332–345, https://doi.org/10.1016/j.energy.2016.11.088.

Arkhipkin, V. S., F. N. Gippius, K. P. Koltermann, and G. V. Surkova (2014), Wind waves in the Black Sea: results of a hindcast study, *Natural Hazards and Earth System Sciences*, *14*(11), 2883–2897, https://doi.org/10.5194/nhess-14-2883-2014.

Aydoğan, B., and B. Ayat (2018), Spatial variability of long-term trends of significant wave heights in the Black Sea, *Applied Ocean Research*, *79*, 20–35, https://doi.org/10.1016/j.apor.2018.07.001.

Battjes, J. A., and J. P. F. M. Janssen (1978), Energy Loss and Set-up Due to Breaking of Random Waves, *Coastal Engineering Proceedings*, *1*(16), 32, https://doi.org/10.9753/icce.v16.32.

Bertin, X., E. Prouteau, and C. Letetrel (2013), A significant increase in wave height in the North Atlantic Ocean over the 20th century, *Global and Planetary Change*, *106*, 77–83, https://doi.org/10.1016/j.gloplacha.2013.03.009.

Bromirski, P. D., D. R. Cayan, J. Helly, and P. Wittmann (2013), Wave power variability and trends across the North Pacific, *Journal of Geophysical Research: Oceans*, *118*(12), 6329–6348, https://doi.org/10.1002/2013jc009189.

Çalışır, E., M. B. Soran, and A. Akpınar (2021), Quality of the ERA5 and CFSR winds and their contribution to wave modelling performance in a semi-closed sea, *Journal of Operational Oceanography*, *16*(2), 106–130, https://doi.org/10.1080/1755876x.2021.1911126.

Camargo, S. J., and A. H. Sobel (2005), Western North Pacific Tropical Cyclone Intensity and ENSO, *Journal of Climate*, *18*(15), 2996–3006, https://doi.org/10.1175/jcli3457.1.

Casas-Prat, M., X. L. Wang, and N. Swart (2018), CMIP5-based global wave climate projections including the entire Arctic Ocean, *Ocean Modelling*, *123*, 66–85, https://doi.org/10.1016/j.ocemod.2017.12.003.

Cavaleri, L., J.-H. Alves, F. Ardhuin, A. Babanin, M. Banner, K. Belibassakis, M. Benoit, M. Donelan, J. Groeneweg, T. Herbers, P. Hwang, P. Janssen, T. Janssen, I. Lavrenov, R. Magne, J. Monbaliu, M. Onorato, V. Polnikov, D. Resio, W. Rogers, A. Sheremet, J. M. Smith, H. Tolman, G. van Vledder, J. Wolf, and I. Young (2007), Wave modelling – The state of the art, *Progress in Oceanography*, *75*(4), 603–674, https://doi.org/10.1016/j.pocean.2007.05.005.

de León, S. P., and C. G. Soares (2015), Hindcast of the Hércules winter storm in the North Atlantic, *Natural Hazards*, *78*(3), 1883–1897, https://doi.org/10.1007/s11069-015-1806-7.

Divinsky, B. V., and R. D. Kosyan (2020), Climatic trends in the fluctuations of wind waves power in the Black Sea, *Estuarine, Coastal and Shelf Science*, *235*, 106,577, https://doi.org/10.1016/j.ecss.2019.106577.

Divinsky, B. V., and S. B. Kuklev (2022), Climate variations of certain wave parameters at the entrance of the Novorossiysk bay, *Oceanology*, *62*(2), 155–161, https://doi.org/10.1134/s0001437022020035.

Dobrynin, M., J. Murawsky, and S. Yang (2012), Evolution of the global wind wave climate in CMIP5 experiments, *Geophysical Research Letters*, *39*(18), 1–6, https://doi.org/10.1029/2012gl052843.

Duan, C., S. Dong, and Z. Wang (2019), Wave climate analysis in the ice-free waters of Kara Sea, *Regional Studies in Marine Science*, *30*, 100,719, https://doi.org/10.1016/j.rsma.2019.100719.

Gippius, F. N., and S. A. Myslenkov (2020), Black Sea wind wave climate with a focus on coastal regions, *Ocean Engineering*, *218*, 108,199, https://doi.org/10.1016/j.oceaneng.2020.108199.

Imrani, Z., S. Safarov, and E. Safarov (2022), Analysis of Wind-wave Characteristics of the Caspian Sea Based on Reanalysis Data, *Russian Meteorology and Hydrology*, *47*(6), 479–484, https://doi.org/10.3103/s1068373922060085.

Ivanov, V. V., V. S. Arkhipkin, E. M. Lemeshko, S. A. Myslenkov, A. V. Smirnov, G. V. Surkova, F. K. Tuzov, D. G. Chechin, and A. A. Shestakova (2022), Changes in hydrometeorological conditions in the Barents sea as an indicator of climatic trends in the eurasian arctic in the 21st century, *Moscow University Bulletin. Series 5: Geography*, (1), 13–25, (In Russian).

Iwasaki, S., and J. Otsuka (2021), Evaluation of Wave-Ice Parameterization Models in WAVEWATCH III Along the Coastal Area of the Sea of Okhotsk During Winter, *Frontiers in Marine Science*, *8*, 1–12, https://doi.org/10.3389/fmars.2021.713784.

Kamranzad, B., A. Etemad-Shahidi, and V. Chegini (2016), Sustainability of wave energy resources in southern Caspian Sea, *Energy*, *97*, 549–559, https://doi.org/10.1016/j.energy.2015.11.063.

Khon, V. C., I. I. Mokhov, F. A. Pogarskiy, A. Babanin, K. Dethloff, A. Rinke, and H. Matthes (2014), Wave heights in the 21st century Arctic Ocean simulated with a regional climate model, *Geophysical Research Letters*, *41*(8), 2956–2961, https://doi.org/10.1002/2014gl059847.

Kislov, A. V., G. V. Surkova, and V. S. Arkhipkin (2016), Occurence frequency of storm wind waves in the Baltic, Black, and Caspian Seas under changing climate conditions, *Russian Meteorology and Hydrology*, *41*(2), 121–129, https://doi.org/10.3103/s106837391 6020060.

Kudryavtseva, N., K. Kussembayeva, Z. B. Rakisheva, and T. Soomere (2019), Spatial variations in the Caspian Sea wave climate in 2002–2013 from satellite altimetry, *Estonian Journal of Earth Sciences*, *68*(4), 225, https://doi.org/10.3176/earth.2019.16.

Lama, G. F. C., T. Sadeghifar, M. T. Azad, P. Sihag, and O. Kisi (2022), On the Indirect Estimation of Wind Wave Heights over the Southern Coasts of Caspian Sea: A Comparative Analysis, *Water*, *14*(6), 843, https://doi.org/10.3390/w14060843.

Lee, H. S., K. O. Kim, T. Yamashita, T. Komaguchi, and T. Mishima (2010), Abnormal storm waves in the winter East/Japan Sea: generation process and hindcasting using an atmosphere-wind wave modelling system, *Natural Hazards and Earth System Sciences*, *10*(4), 773–792, https://doi.org/10.5194/nhess-10-773-2010.

Leo, F. D., S. Solari, and G. Besio (2020), Extreme wave analysis based on atmospheric pattern classification: an application along the Italian coast, *Natural Hazards and Earth System Sciences*, *20*(5), 1233–1246, https://doi.org/10.5194/nhess-20-1233-2020.

Lin-Ye, J., M. García-León, V. Gràcia, M. Ortego, A. Stanica, and A. Sánchez-Arcilla (2018), Multivariate Hybrid Modelling of Future Wave-Storms at the Northwestern Black Sea, *Water*, *10*(2), 221, https://doi.org/10.3390/w10020221.

Liu, Q., A. V. Babanin, S. Zieger, I. R. Young, and C. Guan (2016), Wind and wave climate in the Arctic Ocean as observed by altimeters, *Journal of Climate*, *29*(22), 7957–7975, https://doi.org/10.1175/jcli-d-16-0219.1.

Lopatoukhin, L. I. (2019), Wind wave climate of the Caspian Sea, *Journal of Oceanological Research*, *47*(5), 89–97, https://doi.org/10.29006/1564-2291.jor-2019.47(5).7, (In Russian).

Lopatoukhin, L. I., A. V. Boukhanovsky, A. B. Degtyarev, and V. A. Rozhkov (2003), *Reference data of wind and waves climate of the Barents sea, the sea of Okhotsk, and the Caspian Sea*, 213 pp., Russian Maritime Register of Shipping, Saint-Petersburg.

Lopatoukhin, L. I., A. V. Boukhanovsky, S. V. Ivanov, and E. S. Chernysheva (2006), *Reference data on the regime of wind and waves of the Baltic, Northern, Black, Azov and Mediterranean seas*, 450 pp., Russian Maritime Register of Shipping, Saint-Petersburg.

Lopatoukhin, L. I., A. V. Boukhanovsky, and E. S. Chernysheva (2009), *Reference data on the regime of wind and waves of the sea of Japan and the Kara sea*, 356 pp., Russian Maritime Register of Shipping, Saint-Petersburg.

Lopatoukhin, L. I., A. V. Boukhanovsky, and E. S. Chernysheva (2010), *Reference data on the regime of wind and waves of the Bering and White seas*, 565 pp., Russian Maritime Register of Shipping, Saint-Petersburg.

Lopatukhin, L. I., and N. A. Yaitskaya (2018), Peculiarities of the Approach to Calculation of Wind Waves in the Caspian Sea, *Russian Meteorology and Hydrology*, *43*(4), 245–250, https://doi.org/10.3103/s1068373918040052.

Lyubitskiy, Y. V., A. N. Vrazhkin, and P. O. Kharlamov (2021), Forecasting of hazardous marine hydrometeorological phenomena for the regions of oil and gas deposit development on the Sea of Okhotsk Shelf, *IOP Conference Series: Earth and Environmental Science*, *895*(1), 012,023, https://doi.org/10.1088/1755-1315/895/1/012023.

Mantua, N. J., S. R. Hare, Y. Zhang, J. M. Wallace, and R. C. Francis (1997), A Pacific interdecadal climate oscillation with impacts on salmon production, *Bulletin of the American Meteorological Society*, *78*(6), 1069–1079, https://doi.org/10/b9kgqq.

Maslova, V. N., E. N. Voskresenskaya, A. S. Lubkov, A. V. Yurovsky, V. Y. Zhuravskiy, and V. P. Evstigneev (2020), Intense Cyclones in the Black Sea Region: Change, Variability, Predictability and Manifestations in the Storm Activity, *Sustainability*, *12*(11), 4468, https://doi.org/10.3390/su12114468.

Mei, W., and S.-P. Xie (2016), Intensification of landfalling typhoons over the northwest Pacific since the late 1970s, *Nature Geoscience*, *9*(10), 753–757, https://doi.org/10.1038/ngeo2792.

Morales-Márquez, V., A. Orfila, G. Simarro, and M. Marcos (2020), Extreme waves and climatic patterns of variability in the eastern North Atlantic and Mediterranean basins, *Ocean Science*, *16*(6), 1385–1398, https://doi.org/10.5194/os-16-1385-2020.

Morim, J., C. Trenham, M. Hemer, X. L. Wang, N. Mori, M. Casas-Prat, A. Semedo, T. Shimura, B. Timmermans, P. Camus, L. Bricheno, L. Mentaschi, M. Dobrynin, Y. Feng, and L. Erikson (2020), A global ensemble of ocean wave climate projections from CMIP5-driven models, *Scientific Data*, *7*(1), 105, https://doi.org/10.1038/s41597-020-0446-2.

Myslenkov, S., A. Medvedeva, V. Arkhipkin, M. Markina, G. Surkova, A. Krylov, S. Dobrolyubov, S. Zilitinkevich, and P. Koltermann (2018a), Long-term statistics of storms in the Baltic, Barents and White seas and their future climate projections, *Geography, Environment, Sustainability*, *11*(1), 93–112, https://doi.org/10.24057/2071-9388-2018-11-1-93-112.

Myslenkov, S., M. Markina, V. Arkhipkin, and N. Tilinina (2019), Frequency of storms in the Barents Sea under modern climate conditions, *Moscow University Bulletin. Series 5: Geography*, (2), 45–54, (In Russian).

Myslenkov, S., V. Platonov, A.Kislov, K. Silvestrova, and I. Medvedev (2021a), Thirty-Nine-Year Wave Hindcast, Storm Activity, and Probability Analysis of Storm Waves in the Kara Sea, Russia, *Water*, *13*(5), 648, https://doi.org/10.3390/w13050648.

Myslenkov, S., A. Shestakova, and D. Chechin (2021b), The impact of sea waves on turbulent heat fluxes in the Barents Sea according to numerical modeling, *Atmospheric Chemistry and Physics*, *21*(7), 5575–5595, https://doi.org/10.5194/acp-21-5575-2021.

Myslenkov, S. A., V. S. Arkhipkin, A. V. Pavlova, and S. A. Dobrolyubov (2018b), Wave climate in the Caspian Sea based on wave hindcast, *Russian Meteorology and Hydrology*, *43*(10), 670–678, https://doi.org/10.3103/s1068373918100060.

Myslenkov, S. V., V. S. Arkhipkin, and K. P. Koltermann (2015), Evaluation of swell height in the Barents and White Seas, *Moscow University Bulletin. Series 5: Geography*, (5), 59–66, (In Russian).

Ogorodov, S., D. Aleksyutina, A. Baranskaya, N. Shabanova, and O. Shilova (2020), Coastal erosion of the Russian Arctic: An overview, *Journal of Coastal Research*, *95*(sp1), 599–604, https://doi.org/10.2112/si95-117.1.

Ogorodov, S. A., N. N. Shabanova, A. S. Kessel, A. V. Baranskaya, and S. O. Razumov (2022), Changes of hydrometeorological potential of thermoabrasion on the Russian Arctic coasts, *Moscow University Bulletin. Series 5: Geography*, (1), 26–42, (In Russian).

Onea, F., and L. Rusu (2017), A Long-Term Assessment of the Black Sea Wave Climate, *Sustainability*, *9*(10), 1875, https://doi.org/10.3390/su9101875.

Osipov, A. M., and D. Y. Gushchina (2021), Mechanism of generating two types of EL NIÑO under modern climatic conditions, *Moscow University Bulletin. Series 5: Geography*, (1), 128–135, (In Russian).

Pavlova, A., S. Myslenkov, V. Arkhipkin, and G. Surkova (2022), Storm surges and extreme wind waves in the Caspian sea in the present and future climate, *Civil Engineering Journal*, *8*(11), 2353–2377, https://doi.org/10.28991/cej-2022-08-11-01.

Platonov, V. S., S. A. Myslenkov, V. S. Arkhipkin, and A. V. Kislov (2022), High-resolution modelling of the hydrometeorological fields over the Kara sea coastal regions in complex coastline conditions, *Moscow University Bulletin. Series 5: Geography*, (1), 87–106, (In Russian).

Rusu, L. (2015), Assessment of the wave energy in the Black Sea based on a 15-year hindcast with data assimilation, *Energies*, *8*(9), 10,370–10,388, https://doi.org/10.3390/en80910370.

Rusu, L., S. P. de León, and C. G. Soares (2015), Numerical modelling of the North Atlantic storms affecting the West Iberian coast, in *Maritime Technology and Engineering*, pp. 1365–1370, CRC Press, Taylor & Francis Group, London, https://doi.org/10.1201/b17494-184.

Sasaki, W. (2012), Changes in wave energy resources around Japan, *Geophysical Research Letters*, *39*(23), 1–6, https://doi.org/10.1029/2012gl053845.

Selivanova, J., P. Verezemskaya, N. Tilinina, S. Gulev, and S. Dobrolyubov (2021), The importance of the sea ice marginal zone for the surface turbulent heat fluxes in Arctic on the basis of NCEP CFSR reanalysis, *Russian Journal of Earth Sciences*, *21*(2), 1–8, https://doi.org/10.2205/2020ES000744.

Semedo, A., R. Vettor, Ø. Breivik, A. Sterl, M. Reistad, C. G. Soares, and D. Lima (2014), The wind sea and swell waves climate in the Nordic seas, *Ocean Dynamics*, *65*(2), 223–240, https://doi.org/10.1007/s10236-014-0788-4.

Sharmar, V., and M. Markina (2021), Evaluation of interdecadal trends in sea ice, surface winds and ocean waves in the Arctic in 1980-2019, *Russian Journal of Earth Sciences*, *21*(2), 1–11, https://doi.org/10.2205/2020ES000741.

Shimura, T., and N. Mori (2019), High-resolution wave climate hindcast around Japan and its spectral representation, *Coastal Engineering*, *151*, 1–9, https://doi.org/10.1016/j.coastaleng.2019.04.013.

Shimura, T., N. Mori, and H. Mase (2013), Ocean Waves and Teleconnection Patterns in the Northern Hemisphere, *Journal of Climate*, *26*(21), 8654–8670, https://doi.org/10.1175/JCLI-D-12-00397.1.

Smirnov, V. G., I. A. Bychkova, N. Y. Zakhvatkina, S. V. Mikhal'tseva, and E. V. Platonova (2021), Estimation of the Ice-free Period Length for the Russian Arctic Seas Based on Satellite Data for 2018-2020, *Russian Meteorology and Hydrology*, *46*(10), 683–688, https://doi.org/10.3103/S1068373921100058.

Stefanakos, C. (2021), Global Wind and Wave Climate Based on Two Reanalysis Databases: ECMWF ERA5 and NCEP CFSR, *Journal of Marine Science and Engineering*, *9*(9), 990, https://doi.org/10.3390/jmse9090990.

Stopa, J. E., F. Ardhuin, and F. Girard-Ardhuin (2016), Wave climate in the Arctic 1992–2014: Seasonality and trends, *The Cryosphere*, *10*(4), 1605–1629, https://doi.org/10.5194/tc-10-1605-2016.

Surkova, G. V., and V. A. Romanenko (2021), Seasonal and long-term changes of turbulent heat fluxes between sea and atmosphere in western sector of the Russian Arctic, *Moscow University Bulletin. Series 5: Geography*, (4), 74–82, (In Russian).

Tolman, H. (2019), *User manual and system documentation of WAVEWATCH III version 6.07*, 465 pp., NOAA/NWS/NCEP/MMAB, College Park, MD, USA.

Trenberth, K. E., and J. W. Hurrell (1994), Decadal atmosphere-ocean variations in the Pacific, *Climate Dynamics*, *9*(6), 303–319, https://doi.org/10.1007/BF00204745.

Türkeş, M., and E. Erlat (2018), Variability and trends in record air temperature events of Turkey and their associations with atmospheric oscillations and anomalous circulation patterns, *International Journal of Climatology*, *38*(14), 5182–5204, https://doi.org/10.1002/joc.5720.

Van Vledder, G. P., and A. Akpınar (2015), Wave model predictions in the Black Sea: Sensitivity to wind fields, *Applied Ocean Research*, *53*, 161–178, https://doi.org/10.1016/j.apor.2015.08.006.

Vrazhkin, A. N. (2013), Application of spectral wave model for some areas of the Far Eastern Seas and the Pacific Ocean, *Pacific Oceanography*, *6*(1), 5–9.

Wang, X. L., and V. R. Swail (2001), Changes of extreme wave heights in Northern Hemisphere oceans and related atmospheric circulation regimes, *Journal of Climate*, *14*(10), 2204–2221, https://doi.org/10/dz8fqn.

Waseda, T., A. Webb, K. Sato, J. Inoue, A. Kohout, B. Penrose, and S. Penrose (2018), Correlated increase of high ocean waves and winds in the ice-free waters of the Arctic Ocean, *Scientific Reports*, *8*(1), 1–9, https://doi.org/10.1038/s41598-018-22500-9.

Yaitskaya, N. A. (2017), Retrospective analysis of wind waves in the Caspian Sea in the second half of the XX–beginning of the XXI century and its connection with the regional climate changes, *Geographical bulletin*, (2(41)), 57–70, https://doi.org/10.17072/2079-7877-2017-2-57-70, (In Russian).

Young, I. R., and A. Ribal (2019), Multiplatform evaluation of global trends in wind speed and wave height, *Science*, *364*(6440), 548–552, https://doi.org/10.1126/science.aav9527.

Zieger, S., A. V. Babanin, W. E. Rogers, and I. R. Young (2015), Observation-based source terms in the third-generation wave model WAVEWATCH, *Ocean Modelling*, *96*, 2–25, https://doi.org/10.1016/j.ocemod.2015.07.014.